CORRELATION OF TEXTURE WITH MICROSTRUCTURE IN TWO DUAL PHASE STEELS
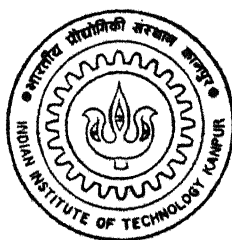
by

Sanjib Kumar Rakshit

Department of Materials and Metallurgical Engineering

INDIAN INSTITUTE OF TECHNOLOGY KANPUR

January, 1996

CORRELATION OF TEXTURE WITH MICROSTRUCTURE IN TWO DUAL PHASE STEELS

A Thesis Submitted
in Partial Fulfilment of the Requirements
for the Degree of

MASTER OF TECHNOLOGY

by

SANJIB KUMAR RAKSHIT

to the

DEPARTMENT OF MATERIALS AND METALLURGICAL
ENGINEERING

INDIAN INSTITUTE OF TECHNOLOGY KANPUR

JANUARY 1996

MME-1996-M-RAC-COR.

**Dedicated
to**
my parents
and
Jhumu

CERTIFICATE

This is to certify that the present work, entitled **Correlation of Texture with Microstructure in Two Dual Phase Steels** by Mr.Sanjib Kumar Rakshit has been carried out under my supervision and it has not been submitted elsewhere for a degree.

Dr. R. K. Ray.
(Professor)

Date :- 29th Jan. 1996

Department of Materials and Metallurgical Engineering.
Indian Institute of Technology.
Kanpur - 208016. India.

ACKNOWLEDGEMENT

SYNOPSIS

Two steels, a plain C and another Nb microalloyed, were investigated in the present work with a view to correlating their textures with microstructures. The steels were subjected to controlled rolling to different finishing temperatures e.g. 1020°C , 850°C , 770°C , 730°C and 630°C. Thereafter, dual phasing treatment was carried out by heating them at two different intercritical temperatures 740° C and 820° C for 3, 15, 30 and 60 minutes followed by water quenching.

Since the deep drawing characteristics of these steels are found to dependent on the orientation of the {111} and {100} planes with respect to the rolling direction, the texture developed during various thermomechanical treatments (**TMT**) is needed to be examined carefully. In order to have a preliminary idea about the textures developed during few selected thermomechanical processing (**TMP**) routes followed by dual phasing treatments, X-ray diffraction analysis was carried out. The integrated X-ray intensity ratios of {222} and {200} peaks were measured from both the rolling and mid plane of each heat treated dual phase structure as well as from the initial controlled rolled samples. Although it has been documented earlier that large volume fractions of martensite are not at all favourable for high {222}/{200} ratios, however, in the present case reasonably high {222}/{200} values (around 1.5) with martensite volume fractions of 40 to 50% have been achieved. Among the various samples, Nb steels controlled rolled at intercritical temperature range $(\alpha + \gamma)$ or at upper ferrite range (α) showed he highest or nearly the highest X-ray intensity ratios.

Quantitative metallography involving measurements of volume fraction of martensite (V^m), number of the martensite particles per unit length (N_l^m), mean random spacing of the martensite particles (σ^m), and mean free path of both the phases e.g. martensite (λ^m) and ferrite (λ^f) were carried out from the **SEM** micrographs. The {222}/{200} intensity ratio was found to increase with the number of martensite particles per unit length (N_l^m) and decrease with the mean random spacing of martensite particles per unit length (σ^m). Again, lower the value of the mean free path of ferrite (λ^f) and martensite (λ^m), higher is the value of the above X-ray intensity ratio.

X-ray line profiles of Mn indicated a slight partitioning of Mn from ferrite to the austenite (martensite) phase. Transmission electron microscopy (**TEM**) studies showed the presence of lath type martensite in case of the plain C steel, whereas both lath type and twinned martensites were found to be present in case of the Nb steel. The presence of dislocated ferrite was revealed in the Nb steel samples whereas they were less abundant in the plain C steel.

CONTENTS

List of Tables

List of Figures

CHAPTER-1

INTRODUCTION

The high strength low alloy (**HSLA**) steels had been extensively used to make the automobile bodies. Although the HSLA steels possess high yield strength, the major drawback of these steels are lack of dynamic stiffness and poor formability. The formability problem of the HSLA steels has been overcome with the introduction of a new type of steel named dual phase steel (around 1975). The microstructure of dual phase steels consists of mainly 80 to 90% soft ferrite with the dispersion of 10 to 20% hard martensite particles. These steels can be produced either by controlling the cooling rate after hot rolling, or by intercritical annealing in the $(\alpha + \gamma)$ range, followed by water quenching so that austenite (γ) transforms to martensite (α').

Compared to the conventional HSLA steels, the dual phase steels show better formability due to their low initial yield strength, continuous yielding behaviour, high work hardening rate right from the beginning of straining and large total elongation before fracture. From the forming limit diagram [Figure 1.1] it can be seen that the dual phase steel (**GM 980X**) is superior to the HSLA steels.

Although dual phase steels are, in general, highly formable, their deep drawability however has been found to be inferior to many low carbon and HSLA steels. This is one of the main disadvantages of such steels. Actually the deep drawability of any sheet steel depends upon the average plastic strain ratio (r_m). The r_m values for the dual phase steels are not so satisfactory. It is known that high r_m value is accompanied by a high value of the $\{222\}/\{200\}$ intensity ratios of X-ray peaks in the material [Figure 1.2]. However, it has been observed that the r_m value of dual phase steels is low relative to the ferrite and ferrite-pearlite steels. This has been attributed mainly to the presence of undesirably oriented martensite particles. Nevertheless, there has been no systematic work yet on the correlation of textures and microstructures in dual phase steels. An attempt has been made in this work to bridge the gap in the existing konowledge in this area. For this purpose, a large number of heat treatment schedules were chosen to produce different volume fractions of martensite in two dual phase steel compositions. X-ray diffraction analysis was carried out on each sample in order to determine the intensity ratios of $\{222\}/\{200\}$ peaks. Further, the microstructure in each sample was evaluated quantitatively and attempts were made to correlate the microstructural parameters as well as martensite contents with the above intensity ratio.

2
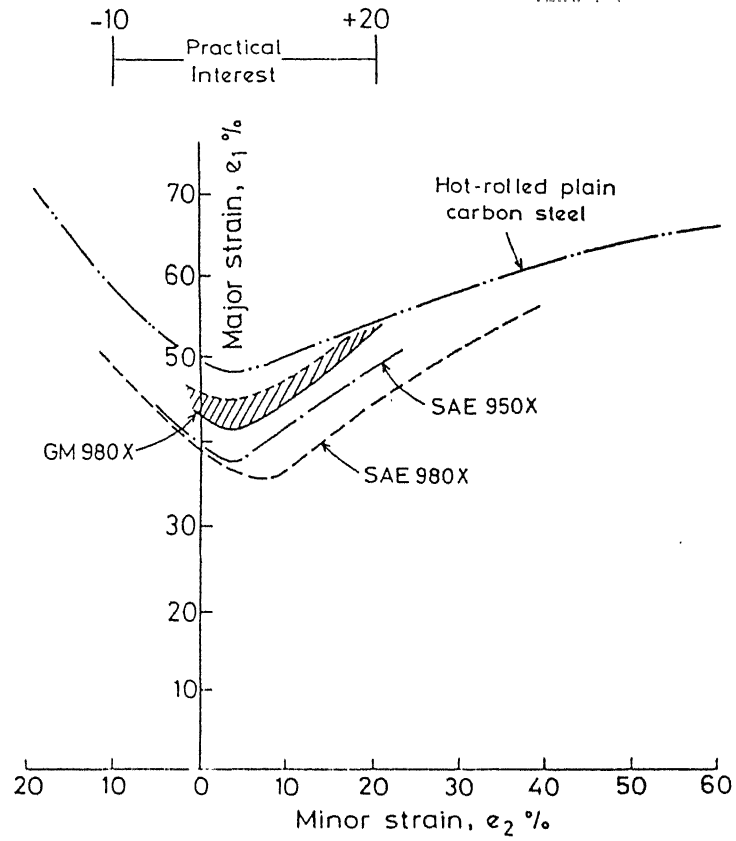
Fig.1.1 Range of the forming limit diagrams (FLD) of dual-phase GM 980X steel compared with that of plain carbon steel and SAE 950X and 980X steels. [45]

Intensity{222}/Intensity{200}
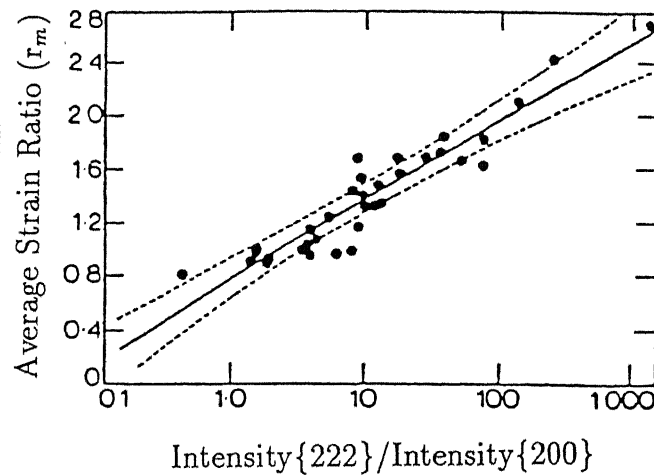
Figure-1.2 Correlation Between r_m and $I_{\{222\}}/I_{\{200\}}$ Texture Ratio in Steels [76].

CHAPTER-2

LITERATURE REVIEW

2.1 Historical Development of Dual Phase Steel

The energy crisis has stimulated the automobile industry to increase car gas mileage. One method would be to reduce the weight of the automobiles. To achieve this end, thinner gauge, high strength material may be employed. Earlier efforts concentrated on the development of high strength steels such as microalloyed controlled rolled, high strength low alloy (HSLA) steels [1,2,3,] or some other variety [4] to meet the above requirements. But it was later found that lack of dynamic stiffness and poor formability are the major problems with HSLA steels. To overcome those problems, more recent developments have led to the commercial production of new type of HSLA steels known as dual phase steels. A new heat treatment approach, defined originally by Japanese workers [5], but later developed in the USA by General Motors (GM) [6] is now followed to produce dual phase steels. These steels consist mainly of 80-90 % polygonal low carbon ferrite and 10-20% of a hard second phase, mostly martensite. Little amount of retained austenite (2-9%) [7] and some amount of low carbon bainite may also be present there as minor constituents. This type of steel is characterised by continuous yielding, high initial work hardening rate, and high value of strain hardening exponent which ultimately gives rise to high uniform elongation and therefore high formability. The heat treatment basically consists of an intercritical annealing treatment *i.e.* reheating the steel strip (either hot rolled or cold rolled) into the austenite-ferrite region of the equilibrium diagram for certain period of time, followed by cooling at such a rate which ensures that the newly formed austenite transforms to martensite.

Hayami and Furukawa [8], first published the results on the superior formability of the Mn bearing dual phase steels on the basis of deep drawability tests. High work hardening and good spot weldability are also obtained alongwith the formability property. Rashid [6] found that high strength dual phase steel with total elongation of as much as 30% can be obtained in GM-980X-V steel which contains very little amount of vanadium and other solid solution hardening elements *e.g.* Mn (1.5%), Si (0.5%). He also has shown that total elongation depends upon the amount of martensite. The tensile strength and the martensite volume fraction (MVF) in dual phase steel have been related by the law of mixture [8,9,10]. The strain hardening parameter n [9] has also been found to depend upon the amount of martensite.

The formation of martensite from austenite totally depends on the chemical composition of the steel *i.e.* its hardenability as well as the rate of cooling. Mn, Si and Cr are generally used to increase the hardenability of the steel. Rashid [6,11] found that

small amount of vanadium as a microalloying element with Mn and Si is sufficient to provide required hardenability. Morrow and coworkers [12-14] got the same effect with the addition of very small amount of molybdenum. Briefly the addition of 0.10-0.75% Mo to a C-Mn-Si steel promotes a dual phase microstructure with continuous yielding, high tensile strength and excellent elongation. But the hardenability of the reformed austenite is a function of the redissolving of the carbonitride precipitates. In steels with small addition of Nb (0.04%), the Nb(C,N) precipitate is so stable at the intercritical annealing (ICA) temperature that the precipitate dose not get dissolved to any great extent [12]. In effect such austenite has low hadenability and the steel exhibits a marked yield point elongation.

Davies [15-18] studied the properties of the dual phase steel produced in a variety of a Fe-Mn-Si-C alloys and observed that the strength of the dual phase steel depends on the ferrite grain size and volume fraction of martensite. A.R.Marder [19] investigated the effect of volume fraction of martensite on the strength, ductility and fracture behaviour of dual phase steels produced from both V and Mo bearing alloys. However, better mechanical properties have been obtained by the addition of V rather than Nb or Mo [12]. With the idea of restricting ferrite grain growth and in order to have sufficient hardenability of the austenite phase during intercritical annealing, the controlled rolled microalloyed HSLA steels are being used as starting material for the production of dual phase steel.

In an alternative method dual phase steel can also be produced by maintaining the appropriate cooling rate just after hot rolling. Coldren and Tither [20] produced dual phase steel from a 0.6%Cr-0.4%Mo-%C alloy following this method. From the C.C.T. diagram [Figure 2.1] developed by them, it is clear that the coiling temperature should be maintained within the coiling window range. The dual phase steel produced thereby has been found to have excellent T.S. and ductility. In Japan [21] also dual phase steel has been produced by dual phase rolling process where low C steel with 0.4%Si-1.4%Mn has been coiled below M_s temperature, thus transforming the austenite to martensite prior to cooling. This process gives inferior tensile strength property in comparison to [20] process.

2.2 Composition of Dual Phase Steel

Mainly dual phase steels are produced from low carbon and low alloy content steels. Generally Mn, Nb, V, Mo, Cr are added to impart sufficient hardenability so that ferrite-carbide aggregate can not be easily formed during cooling from intercritical $(\alpha + \gamma)$ range. Aluminium killed steels having low oxygen and nitrogen content are being used in practice. Also the Japanese are using high silicon steels using Si as a deoxidiser and solid solution strengthening element. Sulphur content is to be as low as possible. Rare earth materials e.g. Zirconium is used for sulphide particle shape control treatment.

The superior properties of dual phase steels e.g. high tensile strength, high formability, enhanced ductility etc. are obtained due to the combination of hard dispersed martensite within the soft ferrite matrix. To obtain ferrite-martensite structure, the

steel should have sufficient hardenability so that martensite can form even at low cooling rate. For this purpose Mn, Si, Cr, Mo, V, Nb, Ti are added in a small range [22,23].

From the point of view of weldability, formability and impact or fracture toughness, the C content should be kept low. The strength is then compensated by increasing Mn content which promotes solid solution strengthening. However, there is a limitation to Mn addition. High Mn content may result in such a depression of transformation temperature of martensite (M_s) that bainite may be formed during cooling. This would impair both the yield stress and the impact properties. That is why Mn content is generally limited to ~1.5% . Besides increasing the hardenability Cr retards the bainite formation. According to Tanaka *et. al.* [24] Cr is the most useful element for dual phase steel production.

The ductility of the overall dual phase structure depends on the cleanliness of the ferrite grains which should possess a finer grain size for maximum strength [16]. For this purpose addition of aluminium is preferred as it removes much of the nitrogen as aluminium nitride. Also AlN in the form of fine dispersed particles causes grain refinement. Grain refinement can also be achieved by small additions of Nb or V, which produce fine precipitates of Nb(CN) and V_4C_3 respectively during transformation [25,26]. Due to higher equilibrium concentration of V than Nb in austenite , V is considered much more effective than Nb [6,12]. V_4C_3 has higher solubility than Nb(CN) at conventional normalising temperature ~950°C. So on normalising Nb steels are only grain refined, whilst V steels are both grain refined and precipitation hardened. Nb steel can only be precipitation hardened if they are heated to higher austenitising temperature [2]. Solid solution strengthening elements *e.g.* Si, Sn and P are considered very effective as a ferrite strengthener [27]. According to Masui and Takechi [28], Si and Mn are the best combination for the purpose of increasing both strength and ductility. Besides increasing hardenability, Mo also has solid solution strengthening effect [29].

Any non metallic inclusion, particularly sulphides (MnS), if present in stringer or tape forms during hot rolling, can be very much detrimental to ductility and toughness. Usually Ca, Zr or Ce (rare earth elements) are used to form rounded globule inclusions rather than elongated tapes or planar arrays. Sometimes Cu can also be used to give an added measure of precipitation strengthening [2]. The initial alloy composition and the volume percentage of martensite in dual phase steel, are to be controlled in such a way that the carbon percentage of martensite is maintained within ~0.3% . This will lead to the formation of lath type martensite, instead of twinned martensite, which suffers from brittleness [30].

2.3 Heat Treatment Cycles

Depending upon the chemical composition of steel, cooling rate may be varied to produce the dual phase microstructure. Just with small addition of alloying elements the hardenability of austenite as well as the cooling rate can be changed in between batch annealing and water quenching for producing martensite. Obviously there must

be a certain difference in physical properties according to the different cooling rates. After all, the dual phase microstructure and its properties are strongly related to the starting structure prior to intercritical annealing, temperature of the intercritical annealing, the holding time and last of all the cooling rate.

The different types of heat treatment cycles used to produce dual phase microstructure are
(a) Intermediate Annealing (I.A.)
(b) Intermediate Normalising (I.N.)
(c) Intermediate Quenching (I.Q.)
(d) Step Quenching (S.Q.)
(e) Continuous Annealing (C.A.)

Steels having coarse and fine ferrite-pearlite initial structure are subjected to intermediate annealing and intermediate normalising cycles respectively. Intermediate quenching is used when the initial structure prior to intercritical annealing is fully martensitic. In step quenching method, the steel sample is held at intercritical range for sometime, from the austenising temperature range and then cooled down to room temperature by a suitable cooling rate. In all the above cases the material is kept at the intercritical annealing temperature for a time interval and then cooled down to ambient temperature by quenching. In the continuous annealing method there is no question of quenching. The hot rolled sheet is coiled in such a manner that the cooling rate during coiling is able to produce dual phase structure. Many investigators simulated the coiling temperature and the coiling condition for this purpose [20,31,32]. Whatever may be the heat treatment cycle, ultimately the steel sample is to be intercritically annealed in between the temperature Ac_1 and Ac_3. These critical temperature are related to the composition of the steel in a way given below [33].

$$Ac_1 = 723 - 10.7Mn - 16.9Ni + 29.1Si + 16.9Cr + 290As + 6.38W \qquad ....(1)$$

$$Ac_3 = 910 - 203\sqrt{C} - 15.2Ni + 44.7Si + 104V + 31.5Mo + 13.1W \qquad ....(2)$$

Depending upon the annealing temperature the volume fraction of austenite pool and its carbon content changes, which affects the hardenability of the austenite. At lower annealing temperature, the hardenability of the austenite pool is higher than at higher annealing temperature [34,35]. The cooling rate dictates the nature of the transformation product of austenite, whether a diffusion controlled product (pearlite or bainite) or a shear transformed product (martensite). A schematic microstructure map showing the volume fraction of various phases present as a function of cooling rate is given in Figure 2.2 [36].

2.4 Effect of Heat Treatment on The Distribution of Phases and the Final Microstructure

The various heat treatment cycles determine the distribution and the morphology of the martensite phase embedded into the soft ferrite matrix. Actually the grain size of the martensite phase is totally dependent on the grain size of the prior austenite grain size before cooling. In case of intermediate annealing or intermediate normalising, dispersed globular martensite is formed along the ferrite grain boundaries. Intermediate quenching is characterised by fine fibrous martensite in the ferrite matrix. In step quenching coarse martensite in the ferrite matrix is obtained.

In general the ferrite grains in dual phase steel are very fine ($\sim 10 \mu$m dia.) because of intercritical annealing of cold rolled sheet metal for shorter time or intercritical annealing of microalloyed steel for longer time. Also the ferrite grains are more or less clean [11,12,14] with significant amount of fine dispersed carbide particles, because, during intercritical annealing, the pearlitic carbide particles go into the solution and get precipitated out in a fine dispersed manner during cooling. Also, after cooling from the intercritical annealing range, some retained austenite (2-9%) and transformed ferrite or new ferrite may be present in the final structure depending upon the influence of the ferrite stabilisers $e.g.$ Si and austenite stabliser $e.g.$ Mn, Cr, V, Mo, etc. Martensite formed from austenite pool may be dislocated (lath) martensite or twinned (acicular) martensite when the carbon percentage of austenite pool is below or above 0.35% respectively. Transmission electron microscopy (TEM) shows the high dislocation density regions in the ferrite matrix adjacent to the martensite islands and the regions of low dislocation density in the ferrite grain interiors [24].

Nakagawa $et.$ $al.$ [37] observed that steels based on Fe-Si-Mn-0.1% C, with V produce discontinuous precipitation of vanadium carbides (V_4C_3) near the ferrite-martensite interface, after ice-brine quench from 800°C temperature, whereas without V no such precipitation was noticed. An uneven distribution of fine precipitates of V(C,N), throughout the ferrite matrix has also been observed in an intercritically annealed V-N steel strip [38]. In case of Nb microalloyed dual phase steels fine precipitation of Nb(C,N) was observed in the retained ferrite region [34]. Those precipitates were found to coarsen with increasing annealing temperature.

From TEM studies [39] on dual phase steel structures produced in a Fe-2% Si-0.1% C alloy by intermediate annealing, intermediate quenching and step quenching it has been shown that there is no remarkable change in the martensite phase. But the formation of subgrains in the ferrite region was observed in case of the intermediate quenched and intermediate annealed structures but not in the step quenched structure. A small quantity (~ 5%) of retained austenite may be present in slowly cooled dual phase steels, especially containing carbide forming elements [40,32,41]. Retained austenite at room temperature is believed to exist in the form of small equiaxed islands rather than thin films [42].

2.5 Mechanical Properties of Dual Phase Steel

2.5.1 Stress Strain Behaviour of Dual Phase Steel

The stress-strain behaviour of dual phase steel [11] is characteristically different from that of ferrite-pearlite steels such as plain carbon or HSLA steel [Figure 2.3]. The ferrite-pearlite steels show the yield point phenomenon, have a high yield to ultimate tensile strength ratio and their strength and ductility (uniform elongation) are inversely related [Figure 2.4]. By contrast, dual phase steels exhibit continuous yielding behaviour, work harden very rapidly at low strains, have a low YS and high UTS and hence a low YS/UTS ratio. They have better formability than the ferrite-pearlite steels of equivalent tensile strength and their strength-ductility data fall on a separate curve [Figure 2.4] from that for ferrite-pearlite steels.

The mathematical expressions which are normally used to the strain hardening behaviour of iron and steel in uniaxial deformation are

$$\sigma = k\epsilon^n \qquad\qquad (Hollomon)~[43] \qquad\qquad ....(3)$$

$$\sigma = \sigma_y + k\epsilon^n \qquad\qquad (Ludwick)~[44] \qquad\qquad ....(4)$$

Here, σ is the true stress, ϵ the true plastic strain, n the work hardening exponent, k the strengthening coefficient and σ_y is the yield stress. The equation (3) has been used to describe the stress-strain behaviour of dual phase steels [45,46], as well as plain carbon and HSLA steels, where a single value of n (work hardening exponent) is assumed. According to the equation (3), the plots of ln σ vs.ln ϵ of the dual phase steel HT-1 (C-0.052%, Mn-0.9%, Si< 0.01%, V< 0.002%, Ti-0.005%) [47], with different volume fraction of martensite (MVF) are clearly not linear [Figure 2.5]. For such alloys which exhibit multiple n behaviour, the analysis suggested by Crussard [48] and Jaoult [49] has been found to be more suitable than Hollomon's analysis. The latter the Ludwick equation mentioned above. According to the Jaoult-Crussard analysis, the Ludwick equation can be re written as

$$\ln~(d\sigma/d\epsilon) = \ln~(kn) + (n\text{-}1)~\ln~\epsilon \qquad\qquad ....~(5)$$

Monterio et. al. [50] have shown that a convenient method for delineating stages in strain hardening is by the application of the Jaoult-Crussard analysis where the plot of ln $(d\sigma/d\epsilon)$ vs.ln ϵ yields several distinct stages of strain hardening during deformation, particularly at low strain.

2.5.2 Strength and Ductility

For the manufacture of automobile components the two important properties of steels are high tensile strength, both for fatigue and crush resistance, and enhanced ductility from the point of view of satisfactory formability. At any strain in the plastic

range, the flow stress of the alloy and the average *in-situ* stresses σ_α and σ_m in ferrite (α) and martensite (m) respectively, are related by the equation (6) given below [51].

$$\sigma_\epsilon = \sigma_\alpha f_\alpha + \sigma_m f_m \qquad \qquad ....(6)$$

where, f_α and f_m are the volume fraction of ferrite and martensite respectively. Rizk and Bourell [52] developed a modified law of mixture equation for dual phase steels.

$$\sigma_c = V_f k_f (\epsilon + \epsilon_{dm})^{n_f} + V_m k_m \epsilon^{n_m} \qquad \qquad .... (7)$$

where,

σ_c = flow stress of the composite (dual phase) material.

ϵ = composite (dual phase) true strain.

k_f, k_m = Hollomon [43] strength coefficients for ferrite and martensite respectively.

n_f, n_m = strain hardening coefficients for ferrite and martensite respectively.

V_f, V_m = volume fractions of ferrite and martensite respectively.

ϵ_{dm} = effective strain in the ferrite due to the austenite to martensite transformation.

The strength of the dual phase steel is linearly proportional to the volume fraction of martensite. The effect of volume fraction of martensite (f_m) on the ultimate tensile strength (UTS) is shown in Figure 2.6 and is represented by the following equation for a Mo and V bearing dual phase steel [53].

$$\text{UTS (MPa)} = 480 + 910 \, f_m \qquad \qquad ....(8)$$

Figure 2.7 shows the effect of f_m on the uniform elongation which is represented by the equation [53]

$$\text{UE(\%)} = (0.23 \text{-} 0.268 \, f_m) \times 100 \qquad \qquad ....(9)$$

Combining the above two equations gives the following equation for uniform elongation and UTS [53].

$$\text{UE(\%)} = 37.2 \text{ - } 0.0295 \text{ UTS}, \qquad \qquad ....(10)$$

which is plotted as a straight line in Figure 2.8. But the strength of the dual phase steel appears to be independent of the carbon content of the martensite [16].

Besides martensite, the mechanical properties of the ferrite matrix must also be considered to arrive at the strength of the composite material. It has been concluded that for optimum properties, the ferrite should be very fine grained ($\sim$3 μ), free of ultra fine carbide precipitates and strengthened by substitutional alloying additions such as Si which minimally affects ductility. On the other hand, addition of P, an effective ferrite stabiliser, does not improve the strength/ductility combinations in dual phase steel. P in ferrite decreases ductility faster than it increases strength [17]. Uniform elongation is used as a measure of ductility, since it is independent of specimen thickness [53]. Superior strength/ ductility combinations imply superior work hardening behaviour. A plot of work hardening rate as a function of strain for a number of conventional and dual phase steels [Figure 2.9] show that the dual phase steels have significantly higher work hardening rate at all strains.

2.6 Sheet Formability

The formability of sheet metals depends to a large extent on their ability to distribute strain. This is characterised by the dimensionless parameter $(1/\sigma)(d\sigma/d\epsilon)$, where σ indicates the instantaneous flow stress value and $(d\sigma/d\epsilon)$ is the instantaneous rate of work hardening. With more and more deformation the material becomes less able to spread the strain to the less deformed parts leading to localised strain concentration and finally ductile fracture by void growth and coalescence [46]. Therefore, for better formability the material should invariably have a high work hardening exponent (n). The material with high work hardening exponent (n) is able to sustain more work hardening which prevents localised strain concentration within the material.

The property of a material which manifests itself in providing different strengths between the plane of the sheet and along the normal of the sheet is called normal anisotropy and the property of having different strengths along different directions in the plane of the sheet itself is termed as planar anisotropy. Both the properties are known as plastic anisotropy. Actually Lankford [54] first suggested the directionality properties which are characterised by the r_m value (also named as plastic strain ratio). It is defined as

$$r_m = (\epsilon_w)/(\epsilon_t) = \frac{ln[(w_o)/(w_f)]}{ln[(t_o)/(t_f)]} \qquad ....(11)$$

where ϵ_w and ϵ_t are the true strain in the width and thickness directions respectively, w_o and w_f are the initial and final width and t_o and t_f are the initial and the final thicknesses. Since most rolled sheets show a variation of elastic and plastic properties with direction in the plane of the sheet, an average strain ratio can be determined by averaging over the strain measured parallel (r_o), transverse (r_{90}) and at 45° (r_{45}) to the rolling direction,

i.e. $r_m = \frac{r_o + 2r_{45} + r_{90}}{4}$ $\qquad ....(12)$

In general it is found that r_0, r_{45} and r_{90} are different for a given sheet material. For this reason earing takes place during deep drawing. Earing can be directly correlated with the planar anisotropy measured by

$$\Delta r = \frac{r_0 + r_{90} - 2r_{45}}{2} \qquad \qquad ....(13)$$

For fully isotropic material r_m would be equal to unity whereas Δr will be equal to zero. The higher the r_m value and lower the $|\Delta r|$ value of the material the higher the resistance to thinning and therefore very desirable for the purpose of deep drawing.

Although the stretch formability of dual phase steel is excellent, the deep drawability is not so good because of the following factors. Firstly, it is difficult to develop the appropriate crystallographic texture necessary for high normal anisotropy (high r_m value). Secondly, it has been observed [55-57] that even when texture is suitable, the hard martensite phase perturbs the deformation of softer ferrite phase and thus reduces the r_m value of the steel. Hatchinson [58] showed that both normal and planar anisotropy are reduced by the presence of martensite constituent. Kurihara et. al. [56] showed that the degradation of the r_m value is dependent on the volume fraction and proximity of the martensite islands and the hardness ratio of martensite and ferrite phase.

2.7 Texture and Its Representation

It is known that for hot rolled, cold rolled or cold rolled and annealed metals or alloys there exists a certain degree of preferred orientation or texture of the grains with respect to some crystallographic planes and directions. Besides microstructures, electronic structures etc., texture is also one of the factors which determines the physical, mechanical and other properties of the material. Texture in rolled sheet metals is generally represented as being of the type {hkl}<uvw>, which means that {hkl} planes of these grains lie parallel to the plane of the sheet, whereas their <uvw> directions lie parallel to the rolling direction.

Texture is conventionally described by means of pole figure, which can be determined by using the appropriate X-ray diffraction techniques. Of course, the pole figure dose not have any meaning unless it contains some reference directions. These are normally taken as some well defined directions in the specimen itself. For example, in case of rolled sheet material the rolling direction (**RD**), transverse direction (**TD**) and the normal direction (**ND**) are usually taken as the reference directions in the corresponding pole figure. Figures 2.10 (a to e) illustrate the procedure for representing texture by pole figures. Detailed description of X-ray method that lead to the determination of pole figures can be found in several texts, *e.g.* by Cullity [59]. For a polycrystalline sample, if the poles are distributed rather uniformly over the area of the projection then there is obviously no texture and the specimen is said to posses a random texture. In practice, however the poles tend to cluster together in certain areas of the pole figure indicating presence of texture [Figure 2.10 (c)]. It is usual to collect orientation data from many grains simultaneously and to present this

in the form of density contours on the pole figures [Figures 2.10 (d and e)].

The informations obtained from pole figures are qualitative and at best semi quantitative. One way of removing this difficulty is to use the crystallite orientation distribution function (**CODF**) or orientation distribution function (**ODF**), which essentially describes the frequency of occurrence of particular orientations in a three dimensional (Euler) orientation space. This space is defined by the three Euler angles, which constitute a set of three consecutive rotations that bring the crystallographic <100> axes of each crystallite into coincidence with the specimen axes *e.g.* RD, TD and ND.

The most widely adopted notations employed for the description of ODFs are those proposed independently by Bunge [60] and by Roe [61]. The Euler angles proposed by Bunge to describe the crystal rotations are ϕ_1, Φ and ϕ_2. The set of angles employed by Roe is referred to as ψ, θ, and ϕ, respectively. These two sets of angles are related as follows [62]

$$\phi_1 = \pi/2 - \psi \qquad \qquad ....(14)$$

$$\Phi = \theta \qquad \qquad ....(15)$$

$$\phi_2 = \pi/2 - \phi \qquad \qquad ....(16)$$

Figure 2.11 shows how, using the Euler angles, the transformation of the sample frame **S** into the crystallite frame **C** occurs by a set of three consecutive reactions namely

(a) A first rotation ϕ_1 around the normal direction ND transforming the transverse direction TD and the rolling direction RD into the new direction TD′ and RD′ respectively. ϕ_1 has to have such a value that RD′ will be perpendicular to the plane formed by ND and [100].

(b) A second rotation Φ around the new direction RD′ with having such a value that ND is transformed into [001] (=ND′) and TD′ into TD″.

(c) A third rotation ϕ_2 around [001] (=ND′) with ϕ_2 having such a value that RD′ is transformed into [100] and TD′ into [010].

The value of the orientation density at each point is simply the strength or intensity of that orientation in multiples of random units. The information contained in a three dimensional ODF in Euler space can be expressed in terms of

(i) **peak** type components that are indicated by pronounced maxima in the ODF.

(ii) **fibre** type components in which a more or less constant intensity is found for a group of orientations related to one another by rotations around a particular crystallographic direction.

It is useful to plot the orientation densities along specific directions or fibres in orientation space, this gives the idea about the texture more quantitatively. The main fibres are shown in Figure 2.12.

These six fibres are defined as follows

(a) RD$_{110}$ fibre, along Φ (0 - 90°) at ϕ_1 = 0° and ϕ_2 = 45° ,

(b) TD$_{110}$ fibre, along Φ (0 - 90°) at ϕ_1 = 90° and ϕ_2 = 45°,

(c) ND$_{111}$ fibre, along ϕ_1 (0 - 90°) at $\Phi = 55°$ and $\phi_2 = 45°$,

(d) ND$_{001}$ fibre, along ϕ_2 (0 - 90°) at $\Phi = 0°$ and $\phi_1 = 0°$,

(e) RD$_{110}$ fibre, along Φ (0 - 90°) at $\phi_1 = 0°$ and $\phi_2 = 0°$,

(f) ND$_{223}$ fibre, along ϕ_1 (0 - 90°) at $\Phi = 45°$ and $\phi_2 = 45°$,

2.8 Textures in Dual Phase Steel

The {111} fibre is particularly beneficial for imparting good deep drawability (high r_m value) to sheet steel, whereas the {001} has a detrimental effect. In practice, the intensity ratio of the above two components $\frac{I_{<111>}}{I_{<100>}}$ is found to approximately linearly related to r_m [Figure 1.2]. The formation of texture in steel is influenced by its alloy chemistry, as well as by the processing parameters, which include the conditions of hot rolling, cold rolling and annealing.

Only a limited amount of work on texture studies in dual phase steel is available in the literature. Dual phase microstructure can be obtained practically in all sheet steels by reheating them in intercritical range followed by cooling to produce a ferrite-martensite phase mixture. Alternatively, these can be produced directly from the rolling heat in hot strip mills. The intercritically annealed dual phase steels are found to exhibit both {111}<uvw> and {337}<uvw> type fibre texture [63], alongwith some minor components such as {310}<001> and {110}<001>. The intensity of the {111}<uvw> components have been reported to be quite moderate, whereas {337}<uvw> components have extremely low intensity. On the other hand, texture components of the type {111}<011>, {111}<112> and {112}<110> have been reported in hot rolled dual phase steels [64]. According to Bunge and Vlad [65], the texture development in dual phase steel grades through hot rolling in the ($\alpha + \gamma$) temperature range is solely governed by the ferrite and its state of recrystallisation and less by the untransformed austenite. It has been observed that, lowering the annealing temperature decreases the r_m value but increases the strength of the steels and vice versa [66]. This is simply because annealing at higher temperature results in further sharpening of the texture through more extensive grain growth.

Ray [67] worked on a C-Mn-Si-V dual phase steel. Cold rolling of this steel by 50% and 70% produced a texture consisting of a moderately strong {111}<112> and rather weak {111}<110> component. Ray and Mondal [68] worked on C-Mn-Si-V dual phase steel, and found that the cold rolled material showed a reasonably strong <111> || ND fibre texture alongwith a weak {11,11,4} fibre and a rather weak and incomplete {337} fibre. The intensities of the {111}<uvw> component have been found to be consistently higher for the material recrystallised at the lower temperature of 650°C as compared to the higher temperature of 800°C.

According to Hu [57], the development of a sufficiently strong {111} texture in a dual phase steel is very difficult because of the undesirably oriented martensite phase, which greatly reduces the r_m value. Hu has shown that a very high r_m value (about 1.8) could be obtained in Si-P steel by producing only a very small quantity ($\sim$ 4 vol.%) of martensite by intercritical annealing, sufficient to eliminate the yield point phenomenon and to increase the initial strain hardening rate.

Unfortunately in dual phase steels, there has not been much systematic work on the correlation between texture and the deep drawing characteristics. It has been observed that both normal and planar anisotropy of dual phase steels are reduced relative to single phase steels having the same crystallographic texture. This behaviour has mostly been attributed to the presence of martensite in the presence of dual phase microstructure. The reason behind this has been the difficulty to achieve a sharp {111} texture in the martensite because of the nature of the γ to α' transformation which has many variants. Even if the ferrite textures could be developed successfully, the undesirably oriented martensite could greatly reduce the r_m value and hence the deep drawing capability. Although it has been shown that very little amount of martensite is desirable in dual phase steels for good deep drawability property [57], it should be remembered at the same time that this will reduce strength of the dual phase steel, which is not at all desirable.

The exact roles played by the amount and distribution of martensite in dual phase steels on the plastic strain ratio can only be found by a detailed and systematic study of the microstructures of the alloys. For this purpose, in the present investigation two different types of steels, one plain C and another Nb microalloyed, were thoroughly studied. Both were controlled rolled by 90% at five different finish rolling temperatures *e.g.* 1020°, 850°, 770°, 730°,and 630°C. Thereafter these were annealed at two different temperatures 740°C and 820°C for different time intervals *e.g.* 3, 15, 30 and 60 minutes. X-ray diffraction analysis was carried out on each sample to determine the intensity ratio of {222} and {200} peaks. SEM micrographs were also taken from all the heat treated samples for the purpose of quantitative evaluation of the microstructures. Attempts were then made to correlate the X-ray intensity ratios with various microstructural parameters.
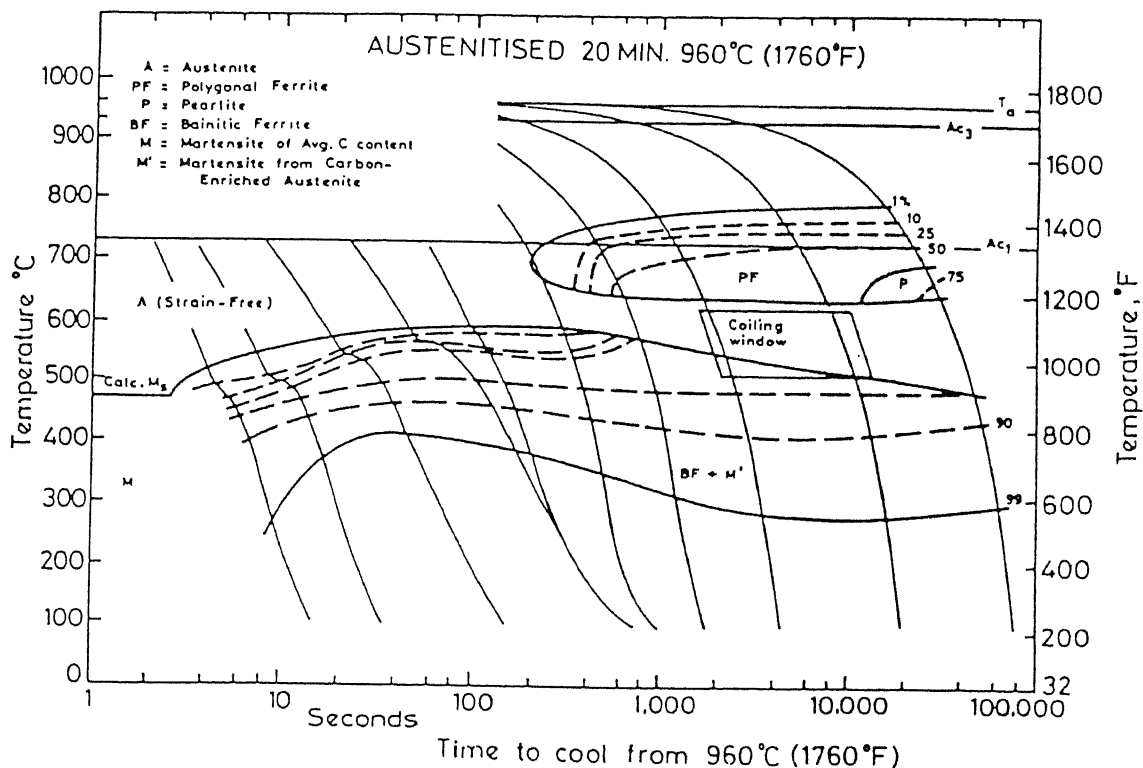
Fig.2.1 C.C.T. curves for a low carbon Mn-Si-Cr-Mo steel developed by Coldren and Tither. [20]
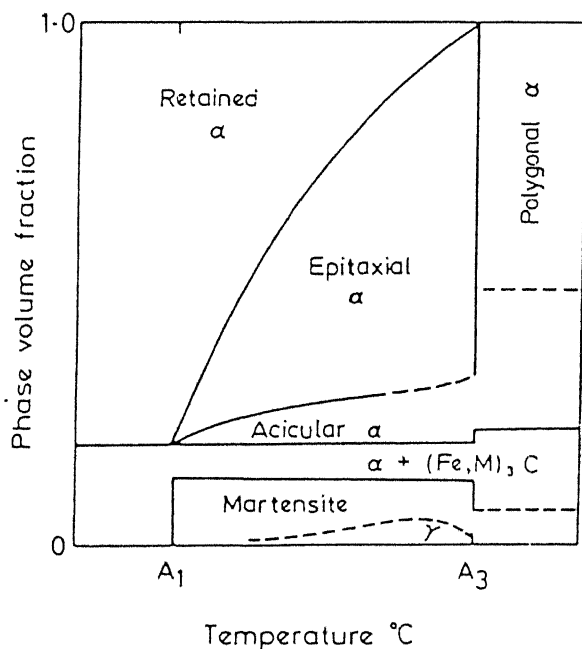
Fig.2.2 Schematic microstructure map showing the volume percent of the various phases present as a function of cooling rate. [36]

Fig.-2.3- Schematic stress-strain curves for plain carbon, HSLA, and dual phase steels. SAE 950X and 980X are Society of Automotive Engineer designations for HSLA steels of different strength levels. GM 980X is General Motors developed dual phase steel. GM 980X is more ductile th SAE 980X although both steels have similar tensile strength. [45]

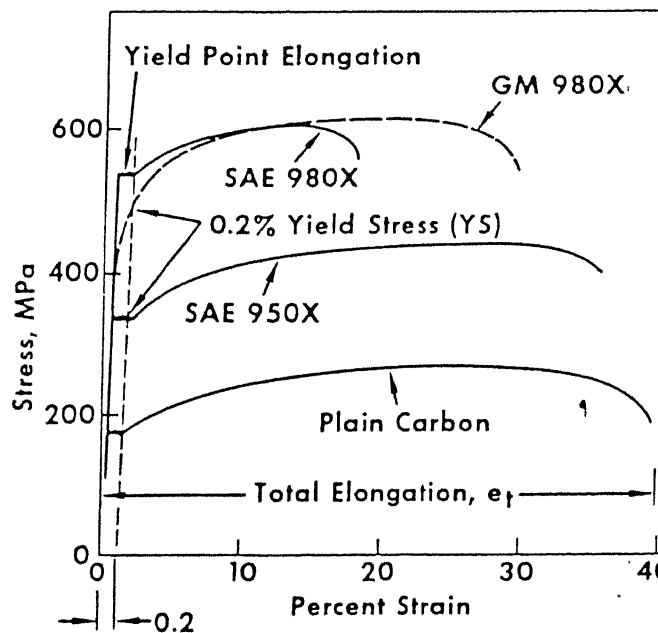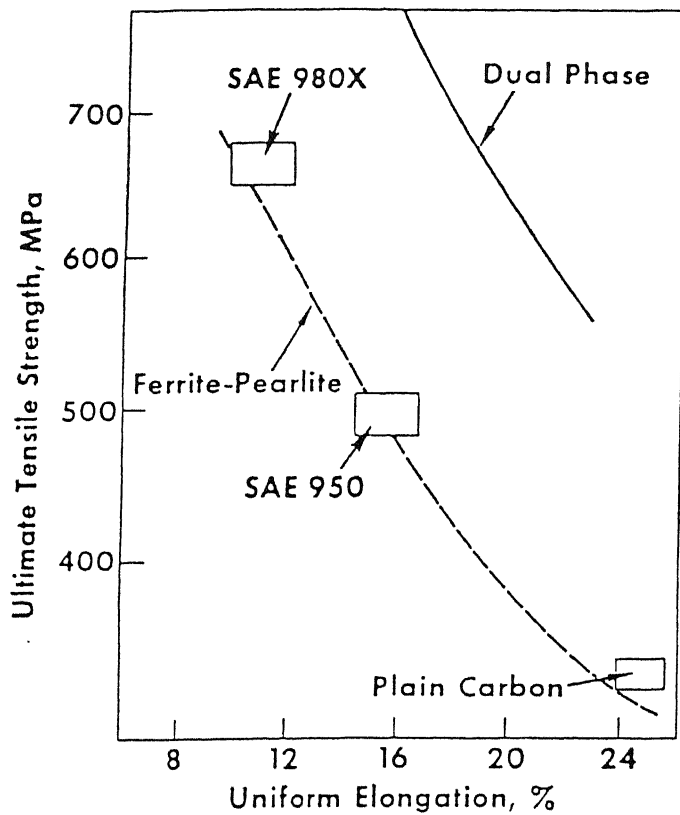Fig.-2.4 – Strength-ductility relationship of dual phase steels compared with that for plain carbon and HSLA steels. The dual phase steel curve is far above that for ferrite-pearlite steels [31]
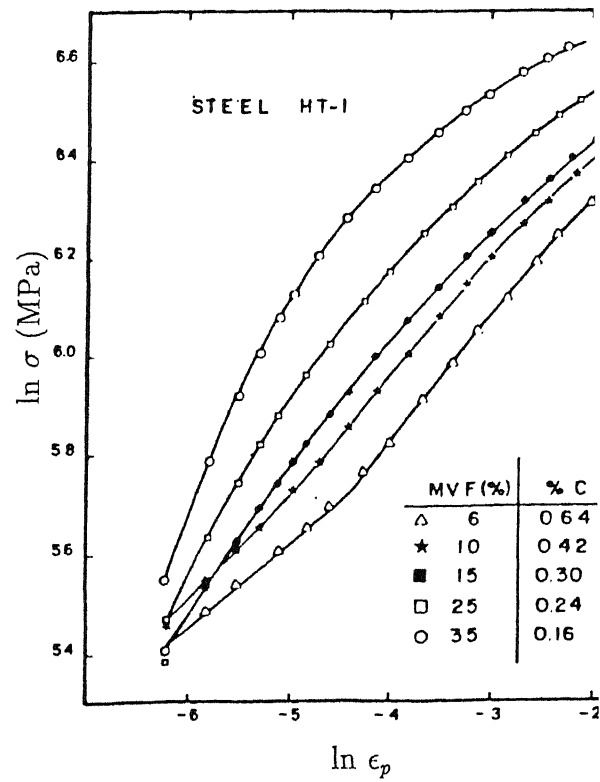
Figure-2.5 Analysis of Stress-Strain Cu of HT-1 According to the Eq.-3 [47
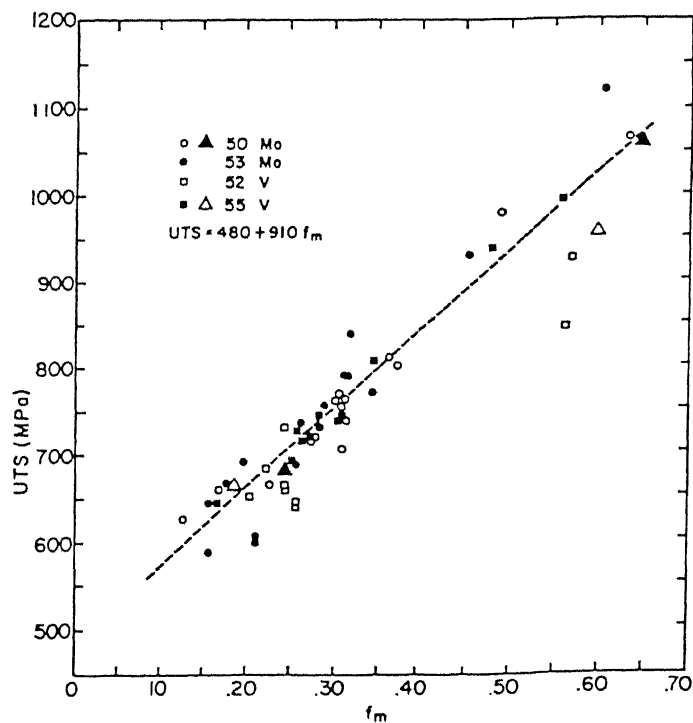
Fig.-2.6 – The effect of volume fraction martensite on the ultimate tensile strength. [19]

%UE = (23 - 0.268 f_m) x 100

○ ▲ 50 Mo
● 53 Mo
□ 52 V
■ △ 55 V

EQUATION 12[4]
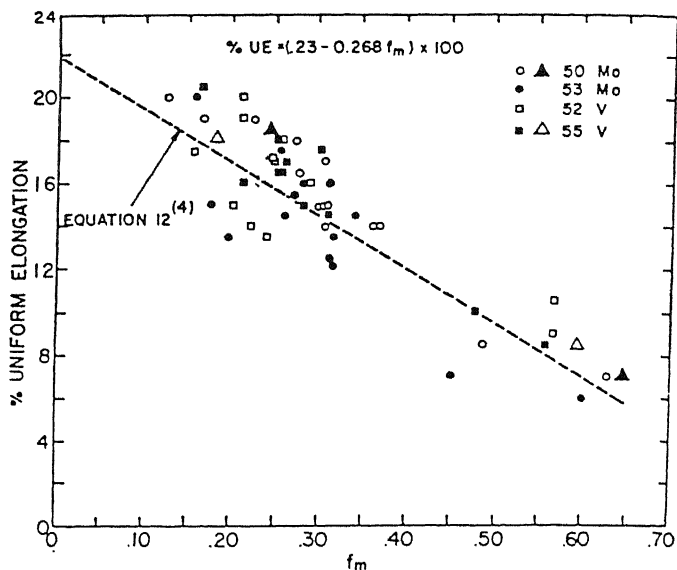
Fig.-2.7—The effect of volume fraction martensite on the uniform elongation. [19]

○ ▲ 50 Mo
● 53 Mo
□ 52 V
■ △ 55 V

%UE = 37.2 - .0295 UTS

Davies[3]

Speich and Miller[4]
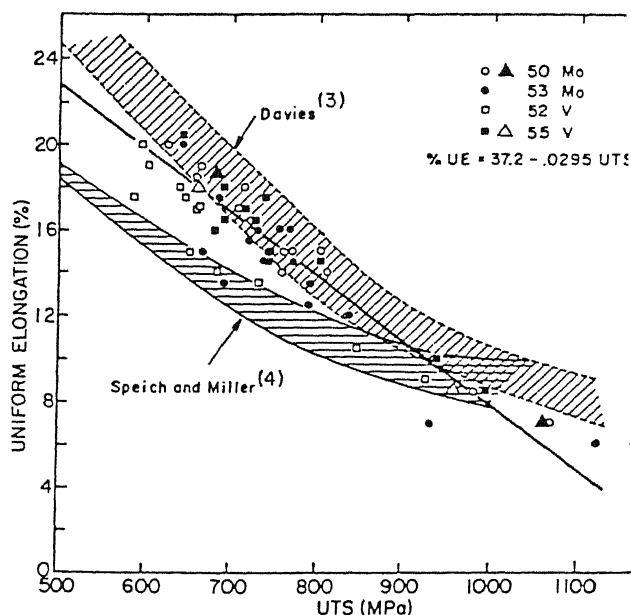
Fig.-2.8·The effect of tensile strength on ductility. [19]

◊ ○ V-Dual-phase as rec.
△ V-Dual-phase q 760°C
□ P-Dual-phase q 760°C
● A K Steel
✦ I F Steel
▲ SAE 950X
■ SAE 980X
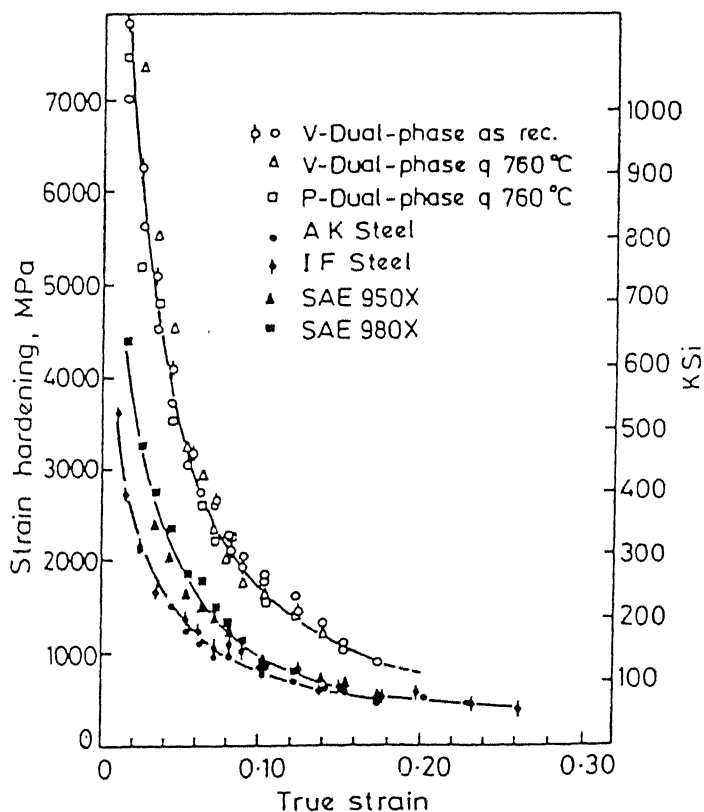
Fig.-2.9-Strain hardening as a function of strain for dual-phase, conventional high strength and low carbon steels.[72]
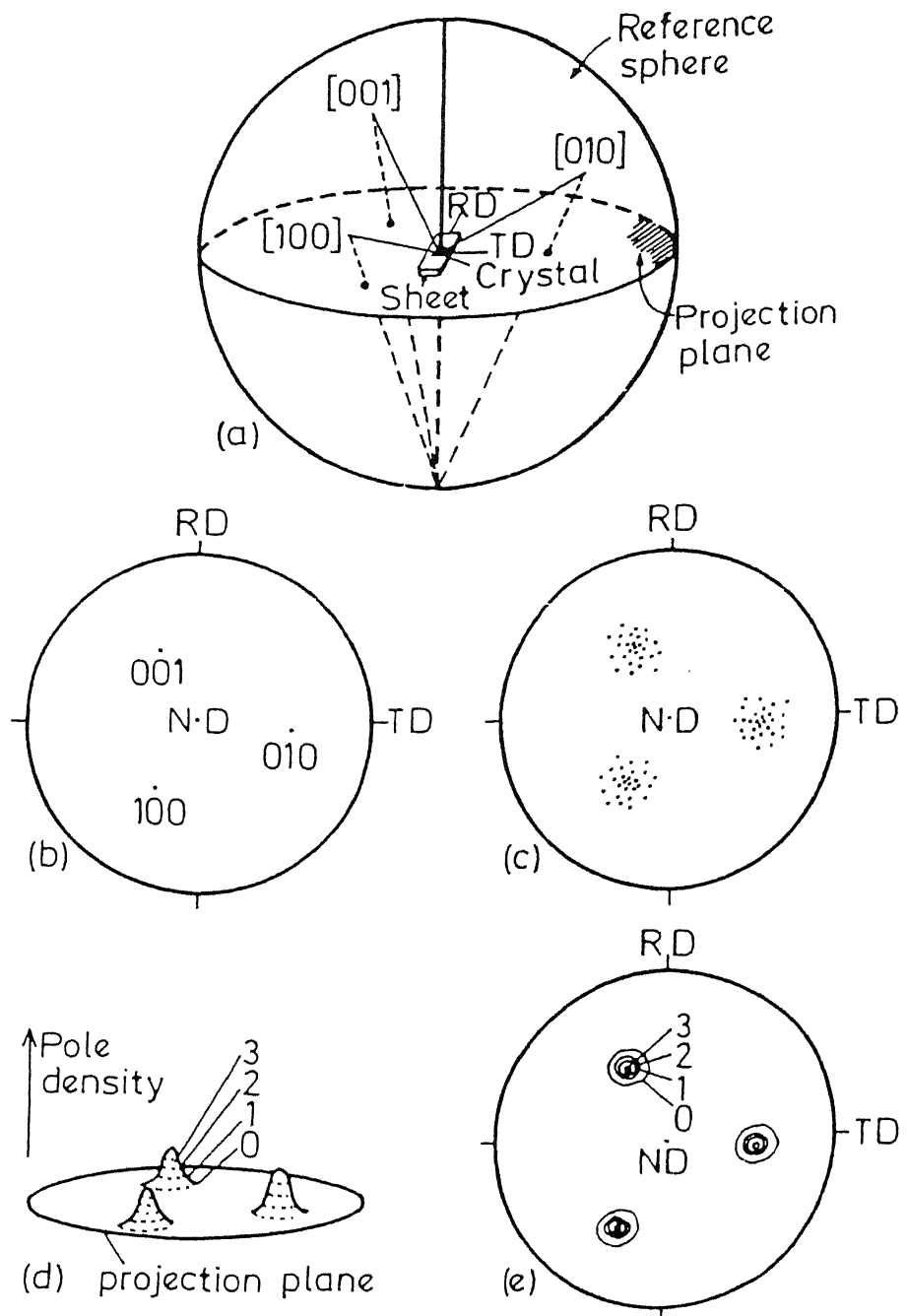
Fig.-2.10-(a) Projection sphere and reference directions,
(b) Projection of poles for a single grain,
(c) Projection of poles from textured grains,
(d) Pole density distribution,
(e) Contour map of pole density. [73]
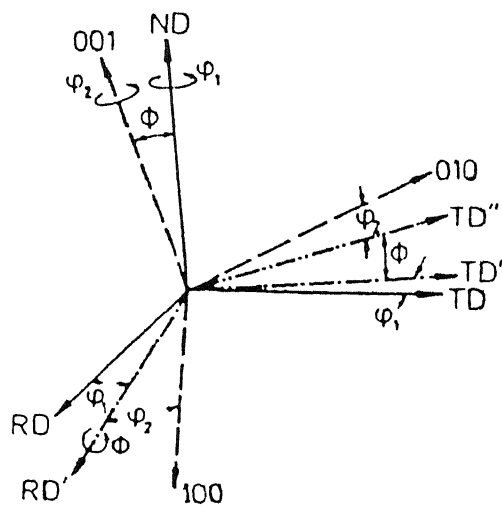
Fig. 2.11 - Defination of the Euler
Angles φ_1, Φ, φ_2 .[74]

Fig.-2.12 **Key depicting the skeleton lines in Euler space**
$(0° \leqslant \phi_1, \Phi, \phi_2 \leqslant 90°)$. .[75]

CHAPTER-3

EXPERIMENTAL PROCEDURE

3.1 Materials and Their Preparation

Two steels, a plain carbon and a Nb microalloyed one were used in the present investigation. The compositions of these steels in wt.% are given below [Table no. 3.1.1].

Table - 3.1.1

Compositions of steels (wt.%)

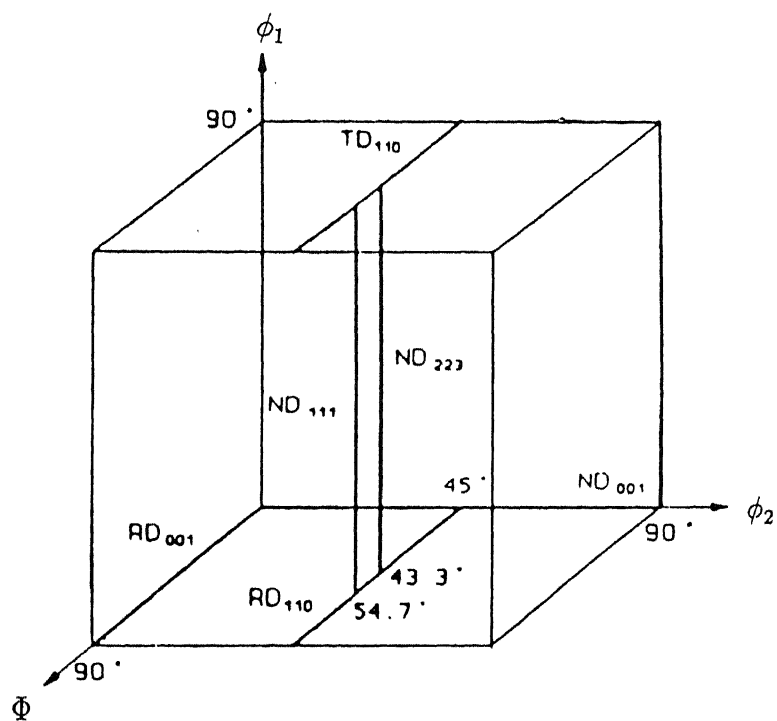|	C	Mn	P	S	Si	V	Nb	ASA[1]	N
Plain C	0.20	1.24	0.011	0.004	0.186	0.004	0.002	0.044	0.0065
Nb steel	0.18	1.35	0.005	0.008	0.244	0.003	0.034	0.048	0.0074

The starting materials were in the form of transfer bars, nearly 50 mm in thickness. These were subjected to controlled rolling to 90% thickness reduction at different finishing temperatures e.g. 1020°, 850°, 770°, 730° and 630°C. Rolling was carried out in a sophisticated research rolling mill at the **CANMET** laboratories in Ottawa, Canada. The final thickness of the rolled plates was 5 mm.

3.2 Dual Phasing Treatment

Before carrying out the dual phasing treatment each rolled plate was cut into eight small pieces of dimension 25mm x 25mm x 5mm. In order to produce the dual phase structure, each sample was heated intercritically for a certain period of time followed by water quenching. Amongst the eight pieces of sample from a particular plate, four were annealed at 740°C temperature for 3, 15, 30 and 60 minutes and the remaining four were annealed at 820°C for the same periods of time (i.e. 3, 15, 30 and 60 minutes). All the above heat treatments were carried out in a tube furnace, where the temperatures were maintained within the range ± 5°C. To prevent the oxidation and decarburisation from the surface, all the heat treatments were done under argon atmosphere. Thus from each starting material eight different dual phase structures were produced.

3.3 Optical Microscopy.

In order to study the effect of rolling on ferrite-pearlite structure microstructures of the initial samples (before dual phasing treatment), were taken from longitudinal sections. These samples were subjected to conventional metallographic polishing and etching by 2% nital (2 ml. concentrated nitric acid in 98 ml. ethyl alcohol). The photomicrographs were taken from the etched surface of each sample in a **LEITZ METALLOVAR** optical microscope. Optical photomicrographs of the dual phase steels showed very poor contrast between the ferrite and martensite particles and thus were not at all suitable for quantitative metallography.

3.4 Scanning Electron Microscopy

For quantitative metallography of the dual phase microstructures scanning electron microscopy (**SEM**) using a **JEOL (JSM - 840A)** scanning electron microscope was carried out on each sample. Either the rolling or the mid planes of samples were examined and this was decided based on the results of the integrated intensity ratios of {222}/{200} peaks, from both the rolling and mid plane of each heat treated dual phase structure. Small pieces of all the samples were mounted separately within cold setting resin for scanning electron microscopy. These mounted samples were subjected to conventional metallographic grinding, polishing and then etching by 2% nital solution. At least five photographs of each sample at different magnifications were taken from different regions of the etched surface using the secondary electron mode. Quantitative metallography was carried out with these photographs. In order to determine the Mn partitioning during heat treatment, between the two phases e.g. ferrite and martensite, the X-ray line profile of Mn was imposed on some selected dual phase microstructures.

3.5 Quantitative Metallography

Multiphase stereology relationships developed by Cribb [69] were used for quantitative analysis of the eighty different dual phase microstructures. To determine the volume percent of martensite, the number of martensite particles per unit length, the mean free path of ferrite and martensite phases and the mean random spacing of martensite particles, the point counting and line intercept measurements were done [69,70] by putting a grid paper (5mm square size) on the printed photographs of different microstructures. For each sample, at least five different photographs taken from different regions were considered and then the average result was taken. The relationships used for the measurements of the above mentioned parameters are given below.

1. $V^m = P_p^m$ where, P_p^f , P_p^m - Point fraction of ferrite and martensite particles respectively.

2. $V^f = P_p^f = 1 - P_p^m$ V^f , V^m - Volume fraction of ferrite and martensite respectively.

3. $\lambda^m = P_p^m / N_l^m$ λ^f , λ^m - Mean free path of ferrite and martensite per unit length respectively.

4. $\lambda^f = P_p^f / N_l^m$ N_l^m - No of the martensite particles per unit length.

5. $\sigma^m = 1 / N_l^m$ σ^m - Mean random spacing of martensite Particles per unit length.

3.6 X-ray Analysis.

Since, the deep drawing characteristics of dual phase steels are found to be dependent on the orientation of {222} and {200} planes the integrated intensity ratios of {222} and {200} peaks, was measured from both the rolling and mid plane of each heat treated dual phase structure. For this purpose, the starting materials and each of the heat treated samples were fine polished on both the rolling and mid planes. This polished samples were subjected to X-ray diffraction studies using Cu K_α radiation in the **SEIFERT ISO DEBYFLEX 2002** X-ray diffractometer. The integrated intensity of each X-ray peak was measured from the area within the individual peaks using 5mm x 5mm transparent grid.

3.7 Transmission Electron Microscopy

A few samples were selected for transmission electron microscopy (**TEM**) on the basis of high intensity ratios of the {222} and {200} peaks. TEM studies were done from the rolling plane of the samples. Initially, the sheets were mechanically thinned down to a thickness of <0.05 mm by polishing on emery paper. A number of 3 mm discs were punched from those thinned samples with the help of a die and a punch. These discs were subjected to electrolytic thinning using a jet polishing device. The electrolyte used for this purpose contained 5 vol.% perchloric acid in glacial acetic acid, kept at the temperature ~10°C. A potential difference of 70 volts and a current of 40 mA was used for electropolishing. Finally, perforated foils with sufficient transparent area (thickness <1000Å) were obtained. These perforated thin foils were rinsed with ethyl alcohol and finally dried. Transmission electron microscopy of the thin foils was carried out in a **JEOL (JEM - 2000 Fx - II)** transmission electron microscope operated at 120 KV.

CHAPTER-4

RESULTS

4.1 As Received Material

As mentioned earlier investigations were carried out on two steels, a plain C and a Nb microalloyed steel. The optical microstructures taken from the longitudinal sections of the as received controlled rolled materials are given in Figure 4.1.1 and Figure 4.1.2 for the plain C and the Nb steel respectively. All the microstructures show aggregates of ferrite and pearlite. In most of the cases the effect of rolling on the microstructures is clearly revealed. In case of samples finish rolled at 1020°C the ferrite and pearlite areas do not show any elongation as in the case for samples finish rolled at lower temperatures. Although, in general there is no major difference in the microstructures of the two steels after comparable controlled rolling, there is a tendency of the grain size of the Nb steel to be a little bit finer than in the plain C steel.

4.2 Results of X-ray Diffraction Analysis

The results of X-ray diffraction analysis for the rolling and the mid planes of each of the samples (as received as well as heat treated ones) are represented in a tabular form in the Tables 4.2.1 to 4.2.5. Table 4.2.1 includes the X-ray diffraction analysis results of as received samples for both the plain C and the Nb steel. Tables 4.2.2 and 4.2.4 contain the results for the the plain C steel subjected to dual phasing at 740°C and 820°C respectively. Tables 4.2.3 and 4.2.5 display the X-ray diffraction results for the Nb microalloyed steels which were annealed at 740°C and 820°C respectively. For the convenience of description a number of plots are also shown in the Figures 4.2.1 to 4.2.3 based on the above results.

The peak intensity ratio of {222}/{200} has been plotted against finish rolling temperature [FRT] for the as received plain C as well as Nb steel from the rolling and mid planes respectively [Figures 4.2.1 (a) and (b)]. It can be seen from these plots that the intensity ratio of {222}/{200} of the plain C steel shows a somewhat higher value than that of the Nb steel, for both the rolling as well as the mid planes. It can also be seen that in most of the cases the finish rolling temperature [FRT] of 730°C gives the highest intensity ratio value. Figures 4.2.2 (a) to (d) show the variation of intensity ratio vs. time of annealing in minutes for the dual phase structures produced from both the plain C and the Nb steel annealed at 740°C. Generally, the X-ray intensity ratios for the rolling plane were found to be higher than those for the

mid plane, in both the steels. Also in most of the cases the steels finish rolled at 770°C (intercritical region) show perceptibly higher intensity ratios (~1.5) after dual phasing treatment. Apart from that, a higher intensity ratio value was also obtained in case of the Nb steel after finish rolling at 630°C and 730°C [Figure 4.2.2 (c)]. The plots in Figures 4.2.3 (a) to (d) show the variation of the intensity ratio, as a function of the finish rolling temperature [FRT] for both the steels, after annealing at 820°C for various lengths of time. Comparing the Figures 4.2.3 (a) and (b) it can be seen that there are no major variations in the intensity ratio plots for the rolling and the mid plane of the plain C steel, whereas for the Nb steel, distinctly higher ratios were obtained for the rolling plane as compared to the mid plane. It is clear from the Figure 4.2.3 (c) that the intensity ratio of {222}/{200} is reasonably high (~1.5) for the Nb steel finish rolled at 770°C and after dual phasing treatment at 820°C for 15 minutes.

4.3 Results of Quantitative Metallography

As stated in section 3.5, all the quantitative measurements were carried out from scanning electron micrographs (SEM) taken in secondary electron mode. To have an idea about the morphological features developed in dual phase steel produced by inter-critical annealing followed by water quenching, a number of SEM microphotographs were taken. Out of those, only two series of typical SEM micrographs are given in Figures 4.3.1 and 4.3.2. Figures 4.3.1 (a) to (j) show the microstructures of the plain C and the Nb steels for all the five FRTs, produced by intercritical annealing at 740°C for 15 minutes. Similarly, Figures 4.3.2 (a) to (j) represent the microstructures of samples which were subjected to annealing at 820°C for 15 minutes. Comparison of the two sets of figures [Figures 4.3.1 and 4.3.2] reveals that the martensite content in the first series is perceptibly less than in the second series. The martensite parti-cles in all the above micrographs appear at a relief from the ferrite background. The martensitic areas are sometimes dispersed and sometimes interconnected. Although any major variation among all the two phase structures [Figures 4.3.1 and 4.3.2] is not apparent, quantitative measurements of some of the parameters mentioned ear-lier, such as volume fraction of martensite (V^m), number of martensite particles per unit length (N_l^m), mean random spacing of martensite particles per unit length (σ^m) and mean free path of the ferrite and martensite particles (λ^f and λ^m respectively) help in bringing out the main difference between the two sets. Tables 4.3.1 to 4.3.4 show the values of all the parameters as a function of heat treatment for the two steels.

Tables 4.3.1 and 4.3.3 contain the results of the quantitative metallography of all the plain C steel samples annealed at 740°C and 820°C respectively, whereas the Tables 4.3.2 and 4.3.4 show the values of the same parameters for all the Nb steel samples annealed at 740°C and 820°C respectively. From these tables [Tables. 4.3.1 to 4.3.4] it can be seen that the volume fraction of martensite (V^m) increases with the holding time for a certain annealing temperature. An exactly opposite tendency could be observed so far as the volume fraction of ferrite (V^f) is concerned. The

number of martensite particles per unit length (N_l^m) decreases with the holding time at a particular annealing temperature. It has also been seen that the mean random spacing of the martensite particles per unit length (σ^m) and the mean free path of martensite (λ^m) both increase gradually with the holding time. The mean free path of ferrite grains (λ^f) decrease with the holding time, but it could not be observed in all the cases.

From Tables 4.2.1 to 4.2.5, the samples which gave the highest or nearly the highest values ($\sim$1.5) of {222}/{200} intensity ratio were located. Their SEM microstructures are presented in Figures 4.3.3 (a) to (f). It was observed that the Nb steels exhibit higher intensity ratios after dual phasing treatment, as compared to the plain C steel. Only in one case in the plain C steel, a reasonably high intensity ratio ($\sim$1.35) was observed. However, it was not as high as in the Nb steel.

To correlate the X-ray intensity ratios with the corresponding microstructural features of the different samples, graphical representations showing the intensity ratio of {222}/{200} peaks vs. different quantitative metallography parameters were prepared. These are shown in Figures 4.3.4 to 4.3.8. From Figure 4.3.4 (a) it can be revealed that in case of plain C steel, there is no clear cut variation in intensity ratio with the volume fraction of martensite. In fact, all the experimental points fall within a band in this case. A slight tendency of the intensity ratio to be higher with the volume fraction of martensite in the range of 35 to 50% can be noticed. Figure 4.3.4 (b) shows that the effect of volume percentage of martensite on the intensity ratio is quite different in the Nb steel as compared to the plain C steel. In the Nb steel reasonably higher intensity ratios ($\sim$1.5) were obtained for a range of volume fraction of martensite around 40 to 55% . In the Nb steel finish rolled at 770°C followed by annealing at 820°C for 15 minutes a higher intensity ratio ($\sim$1.5) could be obtained even though the volume fraction of martensite was around 85% [Tables 4.2.5 and 4.3.4]. Figures 4.3.5 (a) and (b) represent the intensity ratio vs. number of martensite particles per unit length for plain C and Nb steel respectively. From these two figures it is clear that in both the cases the intensity ratio increases as the number of martensite particles per unit length increases. In case of the plain C steel this effect is not as prominent as has been obtained in case of the Nb steel. Figures 4.3.6 (a) and (b) represent, respectively, for the plain C and the Nb steel, the plots of intensity ratio vs. mean random spacing of martensite particles per unit length, which is nothing but the inverse of the number of martensite particles per unit length. In both the cases the intensity ratio increases as the mean random spacing of martensite particles per unit length decreases. This phenomenon is just the opposite to the previous case. This effect is much more predominant in case of Nb steel, as compared to the plain C steel.

From Figures 4.3.7 (a) and (b), it can be seen that the mean free path of martensite per unit length is also a determining factor for the higher intensity ratios. In case of Nb steel [Figure 4.3.7 (b)] this effect is sharper than the plain C steel [Figure 4.3.7 (a)]. The lesser is the value of mean free path of martensite per unit length, higher is the value of intensity ratio. From Figures 4.3.8 (a) and (b) the effect of mean free path of ferrite per unit length on the intensity ratio could be examined. In plain C steel [Figure 4.3.8 (a)] it is not found to be so effective like as in Nb steel [Figure

4.3.8 (b)]. The effect is the same as in the previous case *i.e.* lesser is the mean free path of ferrite higher is the intensity ratio value.

## 4.4 Results of Line Scanning of Dual Phase Structures

It is known that Mn preferentially partitions into the austenite (γ) phase [71]. The temperature for the austenite (γ) to ferrite/martensite (α/α') transformation will be strongly dependent on the amount of Mn in solid solution in austenite (γ). During the dual phasing treatment, specially at higher annealing temperature and for longer holding time, there is a possibility of partitioning of the Mn atoms between the α and γ phases. An attempt was, therefore, made to determine whether there has been significant Mn partitioning during the dual phasing treatment. X-ray line scanning of Mn on both the martensite (from γ) and ferrite phase in a number of heat treated samples was carried out in order to detect the partitioning.

SEM photographs of X-ray line scanning of Mn in a selected number of samples are shown in Figures 4.4.1 to 4.4.4. Figures 4.4.1 (a) to (d) show the Mn partitioning from the ferrite matrix to the martensite (austenite) particles during heat treatment for the plain C steel finish rolled at 1020°C followed by annealing at 740°C for 3 and 60 minutes and at 820°C for 3 and 60 minutes. Similarly, Figures 4.4.2 (a) to (d) represent the X-ray line scanning of Mn for the Nb steel. In both the cases only a slight (if any) partitioning of Mn from ferrite to martensite could be observed. Figures 4.4.3 (a) to (d) and Figures 4.4.4 (a) to (d) show similar results for both the plain C and Nb steel samples. These samples finish rolled at the lower temperature of 630°C also show similar trend *i.e.* a slight (if any) partitioning of Mn from ferrite to martensite for both the plain C (FRT 630°C) and Nb steels (FRT 630°C) where the dual phasing treatments were the same as above.

4.5 Results of Transmission Electron Microscopy

Limited number of TEM photographs were taken from those steel samples (both plain C and Nb) which showed reasonably high value of the {222}/{200} X-ray intensity ratios. Figures 4.5.1 (a) and (b) show the TEM microstructures of the general features for the plain C steel, finish rolled at 770°C and annealed at 740°C for 15 minutes, and for the Nb steel finish rolled at 770°C followed by the same heat treatment mentioned above. For plain C steel, as it can be seen from Figure 4.5.1 (a), the dislocations in the ferrite areas adjacent to the martensite particles are not as abundant as observed in case of the Nb steel [Figure 4.5.1 (b)]. Figures 4.5.2 (a) and (b) represent two TEM microstructures from two different areas of the Nb steel, finish rolled at 730°C followed by annealing at 740°C for 15 minutes. The highly dislocated ferrite areas adjacent to the martensitic region is shown in Figure 4.5.2 (a).It can be observed that some of the dislocation lines are arranged parallel to one another. Figure 4.5.2 (b) shows that the martensite in this case is internally twinned showing mid ribs. Figures 4.5.3 (a) and (b) show the TEM features from the Nb steel,
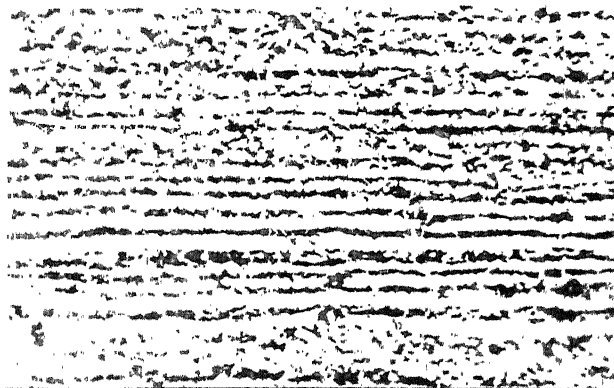
finish rolled at 770°C followed by annealing at 820°C for 15 minutes and from the plain C steel, finish rolled at 630°C, followed by annealing at 820°C for 30 minutes, respectively. In both the cases the martensite was found to be of the lath type. Thus, the Nb steel exhibited both types of martensite - internally twinned as well as lath type.
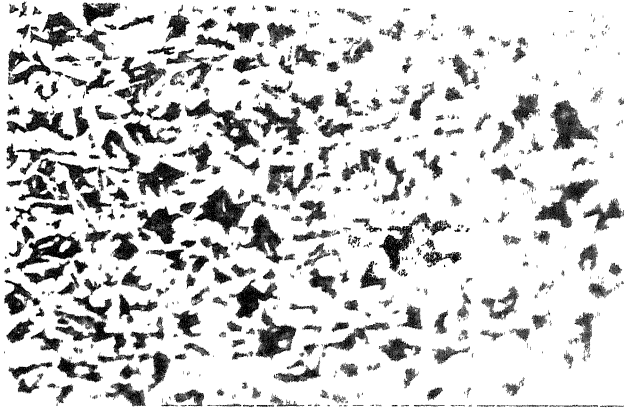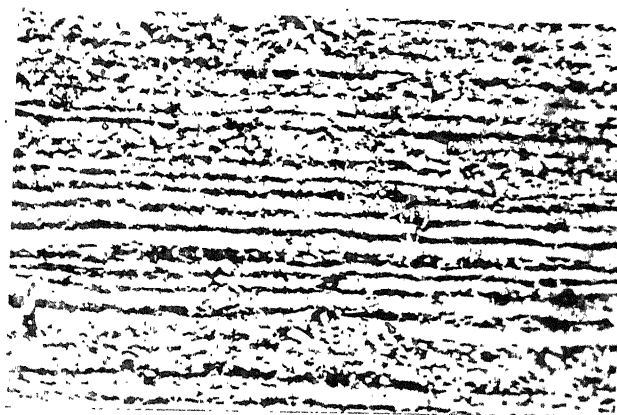
(a)   **200X**

(b)   **200X**

(c)   **200X**
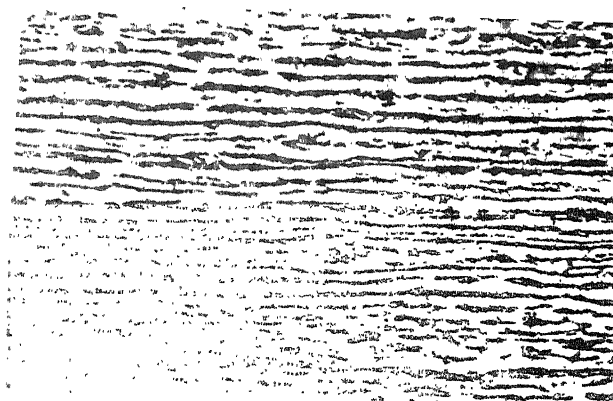
Figure-4.1.1 Optical Microstructures of the As Received Plain C Steel
(a) FRT - 1020°C.
(b) FRT - 850°C.
(c) FRT - 770°C.

29

(d)   · **200X**

·(e)   **200X**

Figure-4.1.1 Optical Microstructures of the As Received Plain C Steel
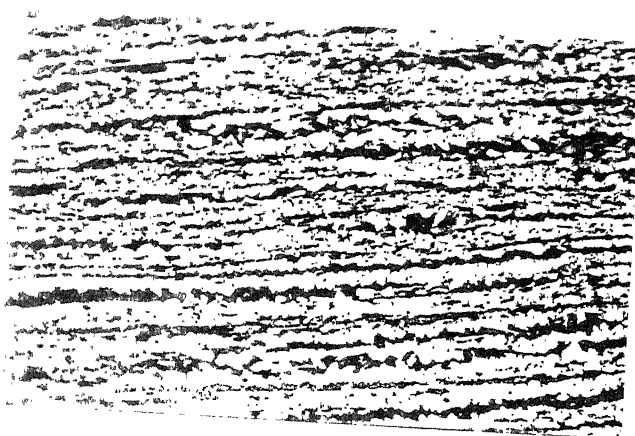(d) FRT - 730°C.
(e) FRT - 630°C.

(a)   200X
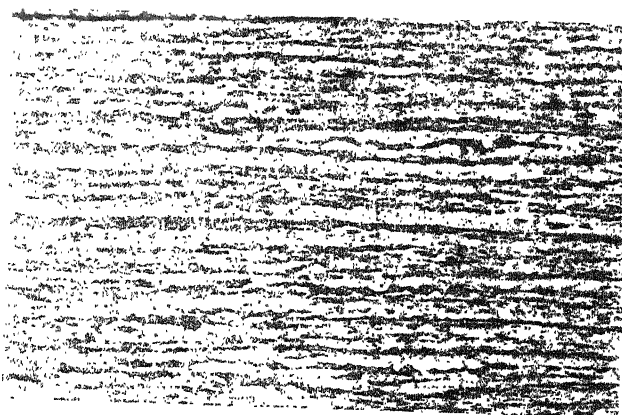

(b).   200X
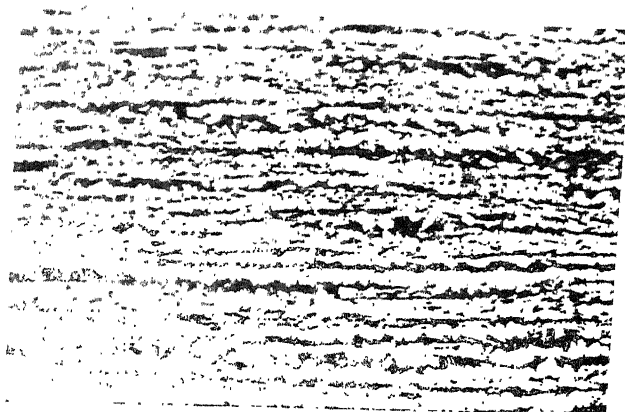
(c)   200X

Figure-4.1.2 Optical Microstructures of the As Received Nb Steel
(a) FRT - 1020°C.
(b) FRT - 850°C.

(d)   200X

(e)   200X

Figure-4.1.2 Optical Microstructures of the As Received Nb Steel
(d) FRT - 730°C.
(e) FRT - 630°C.

TABLE - 4.2.1

Material	Finish Rolling Temperature (°C)	{222}/{200} Intensity Ratio on Rolling Plane	{222}/{200} Intensity Ratio on Mid Plane
Plain C Steel	1020°C	0.71	0.82
	850°C	0.60	0.93
	770°C	0.58	0.90
	730°C	0.86	0.95
	630°C	0.39	0.62
Nb Steel	1020°C	0.65	0.69
	850°C	0.54	0.67
	770°C	0.45	0.49
	730°C	0.47	0.76
	630°C	0.59	0.69

{222}/{200} Intensity Ratios for the
Two Steels in the As-Received Condition.

TABLE - 4.2.2

As Received Sample	Heat Treatment Schedules	{222}/{200} Intensity Ratio on Rolling Plane	{222}/{200} Intensity Ratio on Mid Plane
Plain C Steel Finish Rolled at 1020°C	740°C/3 mins.	0.70	0.58
	740°C/15 mins.	0.63	0.50
	740°C/30 mins.	0.74	0.67
	740°C/60 mins.	0.65	0.72
Plain C Steel Finish Rolled at 850°C	740°C/3 mins.	1.00	0.94
	740°C/15 mins.	0.69	0.82
	740°C/30 mins.	0.60	0.60
	740°C/60 mins.	0.18	0.85
Plain C Steel Finish Rolled at 770°C	740°C/3 mins.	0.87	0.86
	740°C/15 mins.	1.35	0.99
	740°C/30 mins.	1.10	0.80
	740°C/60 mins.	0.33	0.56
Plain C Steel Finish Rolled at 730°C	740°C/3 mins.	0.88	0.85
	740°C/15 mins.	0.52	0.54
	740°C/30 mins.	0.57	0.70
	740°C/60 mins.	0.71	0.69
Plain C Steel Finish Rolled at 630°C	740°C/3 mins.	1.00	0.95
	740°C/15 mins.	0.47	0.60
	740°C/30 mins.	0.70	0.52
	740°C/60 mins.	0.72	0.50

{222}/{200} Intensity Ratios for the Plain C Steel
in the Heat Treated Condition *(Annealing Temperature 740 °C)*.

TABLE - 4.2.3

| As Received Sample	Heat Treatment Schedules	{222}/{200} Intensity Ratio on Rolling Plane	{222}/{200} Intensity Ratio on Mid Plane
Nb Steel Finish Rolled at 1020°C	740°C/3 mins.	0.53	0.73
	740°C/15 mins.	0.54	0.52
	740°C/30 mins.	0.62	0.56
	740°C/60 mins.	0.55	0.67
Nb Steel Finish Rolled at 850°C	740°C/3 mins.	0.49	0.58
	740°C/15 mins.	0.64	0.56
	740°C/30 mins.	0.72	0.61
	740°C/60 mins.	0.51	0.67
Nb Steel Finish Rolled at 770°C	740°C/3 mins.	0.37	0.60
	740°C/15 mins.	1.50	0.53
	740°C/30 mins.	0.56	0.67
	740°C/60 mins.	1.50	0.68
Nb Steel Finish Rolled at 730°C	740°C/3 mins.	0.50	0.54
	740°C/15 mins.	1.55	0.39
	740°C/30 mins.	0.53	0.75
	740°C/60 mins.	0.93	0.78
Nb Steel Finish Rolled at 630°C	740°C/3 mins.	1.48	0.52
	740°C/15 mins.	0.98	0.66
	740°C/30 mins.	0.83	0.68
	740°C/60 mins.	1.00	0.57

{222}/{200} Intensity Ratios for the Nb Steel
in the Heat Treated Condition *(Annealing Temperature 740 °C)*.

TABLE - 4.2.4

As Received Sample	Heat Treatment Schedules	$\{222\}/\{200\}$ Intensity Ratio on Rolling Plane	$\{222\}/\{200\}$ Intensity Ratio on Mid Plane
Plain C Steel Finish Rolled at 1020°C	820°C/3 mins.	0.50	0.54
	820°C/15 mins.	0.58	0.65
	820°C/30 mins.	0.57	0.45
	820°C/60 mins.	0.45	0.55
Plain C Steel Finish Rolled at 850°C	820°C/3 mins.	0.33	0.76
	820°C/15 mins.	0.51	0.55
	820°C/30 mins.	0.55	0.47
	820°C/60 mins.	0.64	0.52
Plain C Steel Finish Rolled at 770°C	820°C/3 mins.	1.00	0.77
	820°C/15 mins.	1.00	0.65
	820°C/30 mins.	0.39	0.72
	820°C/60 mins.	1.01	0.60
Plain C Steel Finish Rolled at 730°C	820°C/3 mins.	0.70	0.65
	820°C/15 mins.	0.59	0.60
	820°C/30 mins.	0.56	0.56
	820°C/60 mins.	0.43	0.79
Plain C Steel Finish Rolled at 630°C	820°C/3 mins.	0.50	0.47
	820°C/15 mins.	0.70	0.95
	820°C/30 mins.	0.88	1.00
	820°C/60 mins.	0.97	0.67

$\{222\}/\{200\}$ Intensity Ratios for the Plain C Steel
in the Heat Treated Condition *(Annealing Temperature 820 °C)*.

TABLE - 4.2.5

As Received Sample	Heat Treatment Schedules	{222}/{200} Intensity Ratio on Rolling Plane	{222}/{200} Intensity Ratio on Mid Plane
Nb Steel Finish Rolled at 1020°C	820°C/3 mins.	0.43	0.64
	820°C/15 mins.	0.50	0.45
	820°C/30 mins.	0.48	0.55
	820°C/60 mins.	0.50	0.50
Nb Steel Finish Rolled at 850°C	820°C/3 mins.	0.77	0.66
	820°C/15 mins.	0.75	0.58
	820°C/30 mins.	0.53	0.52
	820°C/60 mins.	0.47	0.64
Nb Steel Finish Rolled at 770°C	820°C/3 mins.	0.88	0.64
	820°C/15 mins.	1.50	0.67
	820°C/30 mins.	0.84	0.65
	820°C/60 mins.	0.65	0.53
Nb Steel Finish Rolled at 730°C	820°C/3 mins.	0.73	0.55
	820°C/15 mins.	1.05	0.64
	820°C/30 mins.	0.44	0.52
	820°C/60 mins.	0.83	0.80
Nb Steel Finish Rolled at 630°C	820°C/3 mins.	1.02	0.55
	820°C/15 mins.	0.80	0.88
	820°C/30 mins.	0.50	0.82
	820°C/60 mins.	0.53	0.74

{222}/{200} Intensity Ratios for the Nb Steel
in the Heat Treated Condition *(Annealing Temperature 820 °C)*.
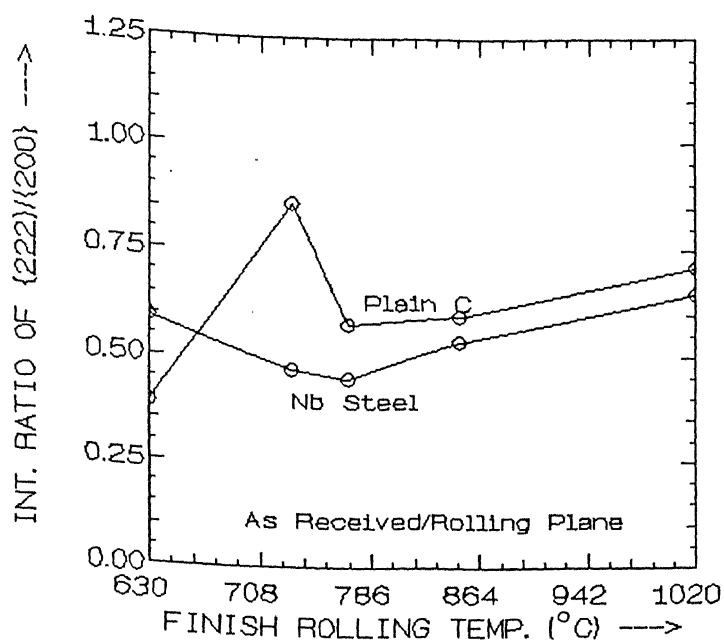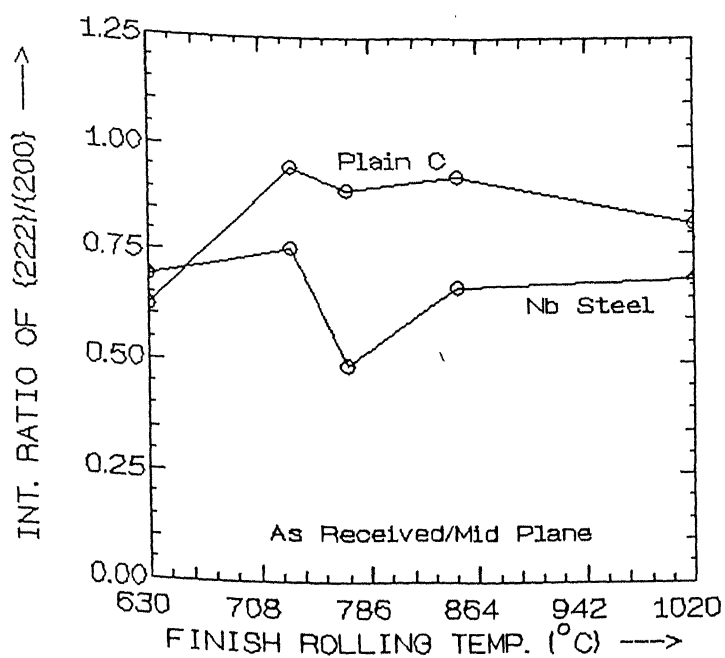
Figure-4.2.1 {222}/{200} Intensity Ratio vs. Finish Rolling Temp.(FRT)
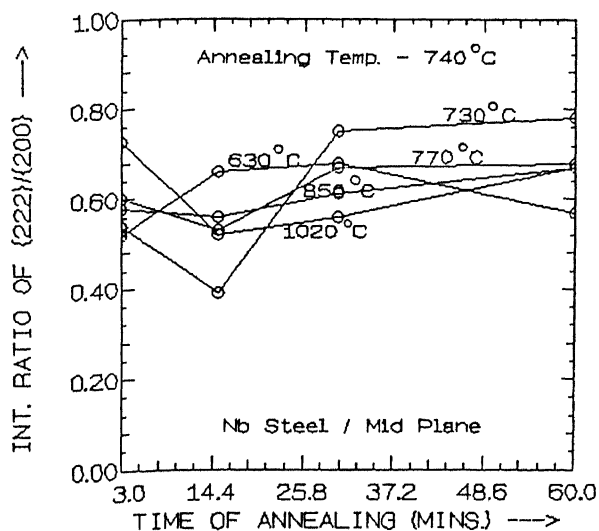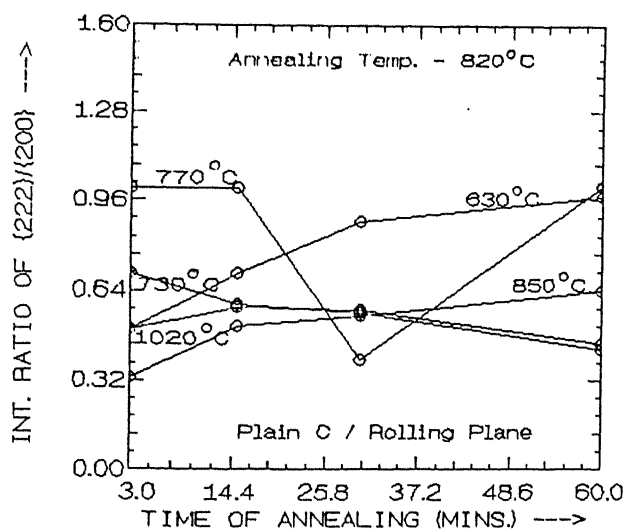for both the As Received Materials.
(a) Rolling Plane
(b) Mid Plane
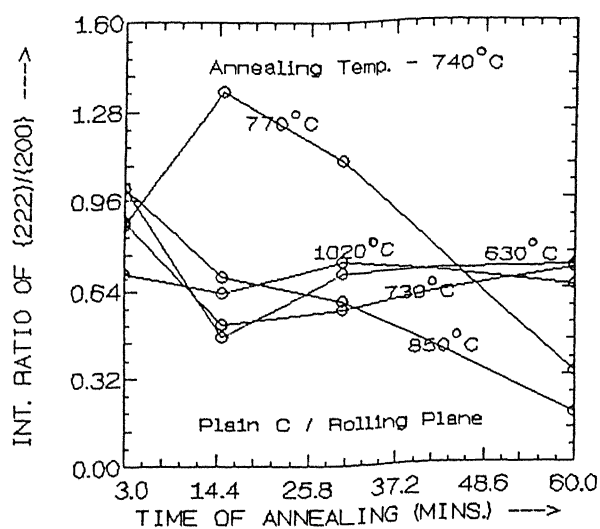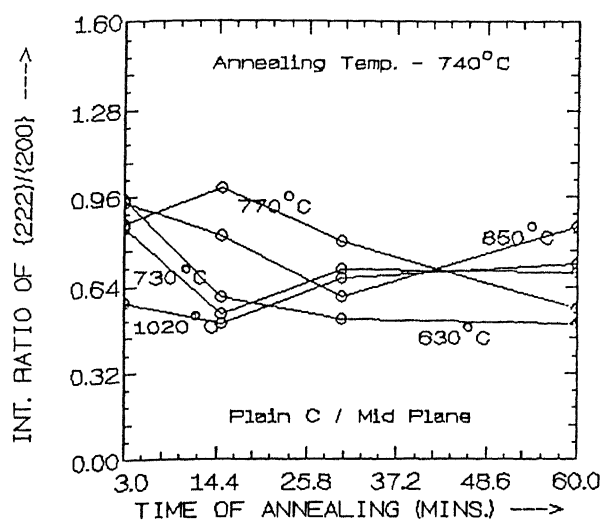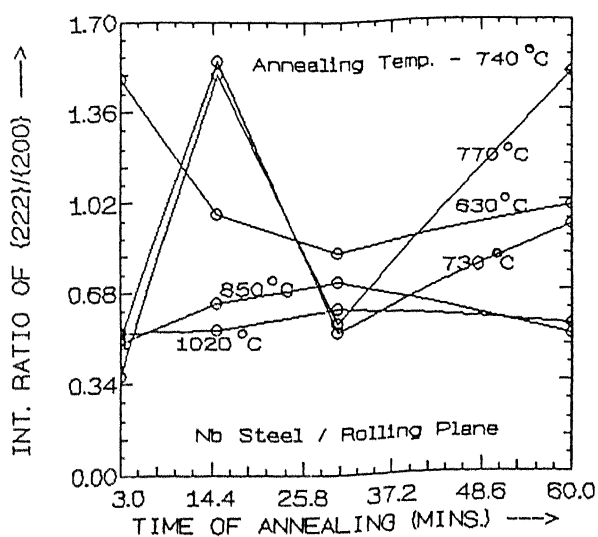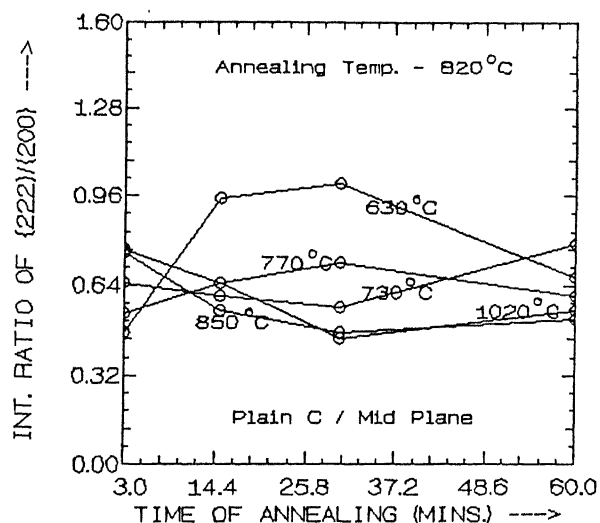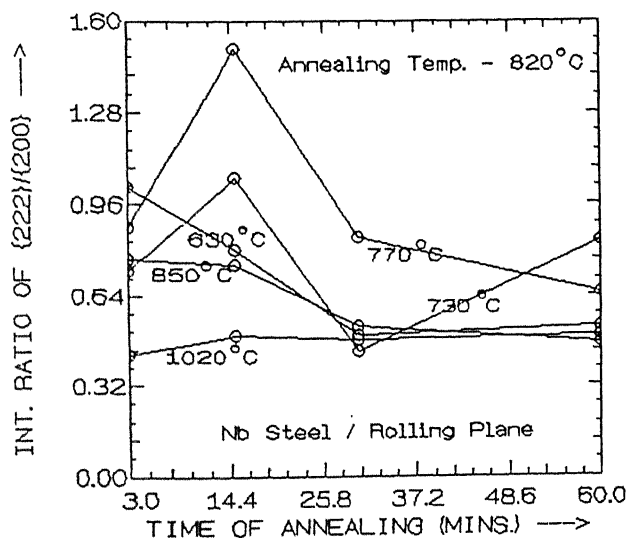
Figure-4.2.2 {222}/{200} Intensity Ratio vs. Time of Annealing at 740°C for
(a) Plain C/Rolling Plane
(b) Plain C/Mid Plane
(c) Nb Steel/Rolling Plane
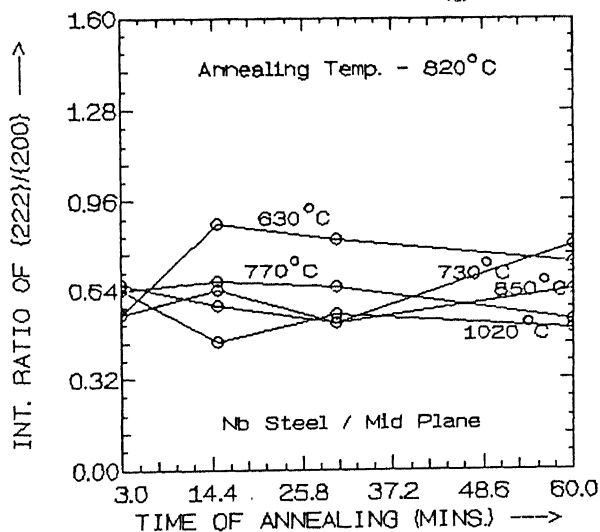(d) Nb Steel/Mid Plane
for all Five FRTs.

Figure-4.2.3 {222}/{200} Intensity Ratio vs. Time of Annealing at 820°C for
(a) Plain C/Rolling Plane
(b) Plain C/Mid Plane
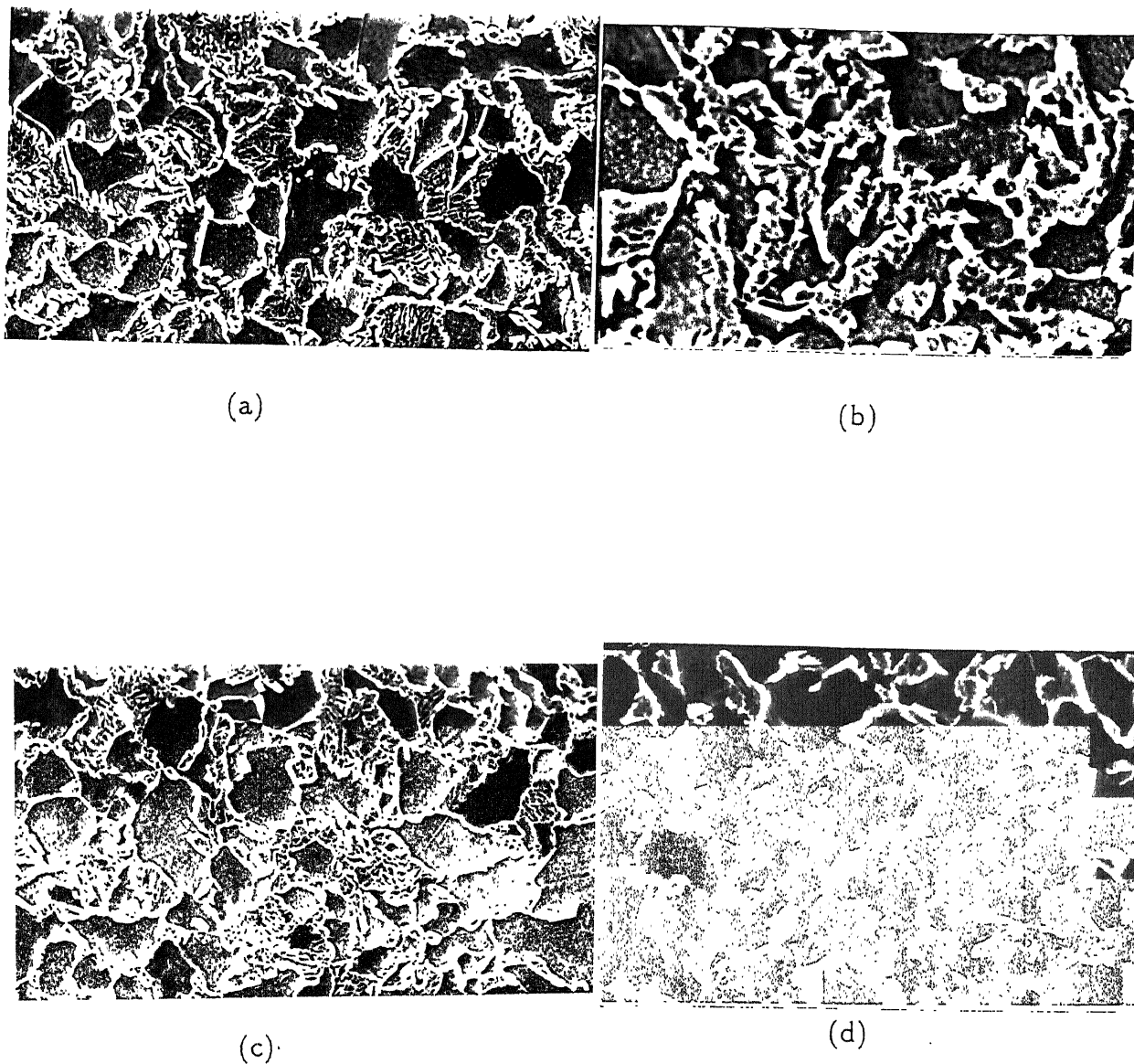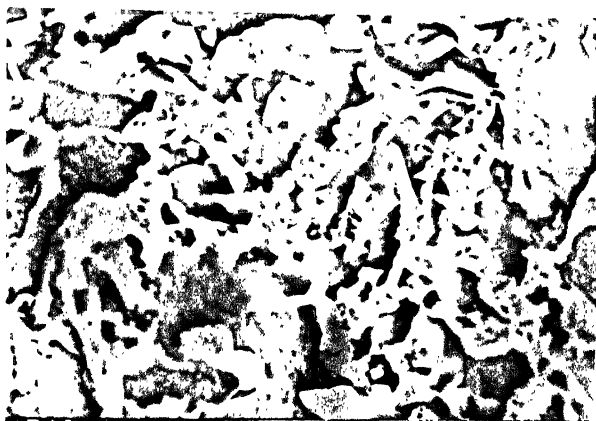(c) Nb Steel/Rolling Plane
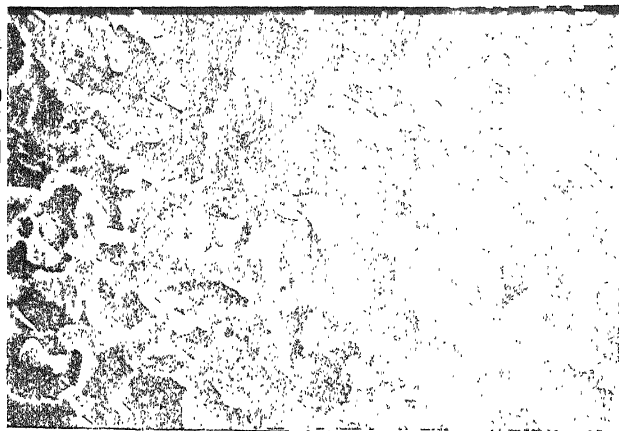(d) Nb Steel/Mid Plane
for all Five FRTs.

(a)

(b)

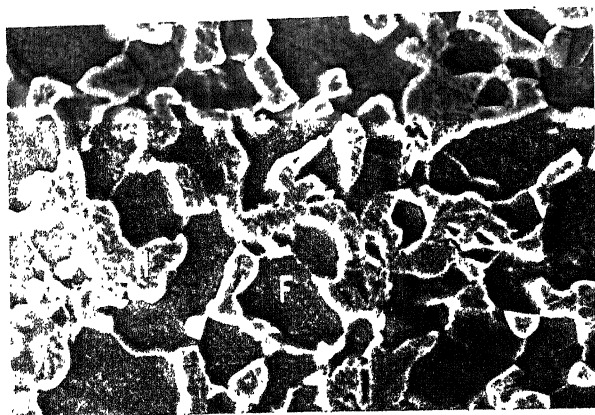(c)·

(d)

Figure-4.3.1 SEM Micrographs of Plain C and Nb Steels

(a) Plain C/FRT 1020°C/Annealed at 740°C for 15 minutes.
(b) Nb Steel/FRT 1020°C/Annealed at 740°C for 15 minutes.
(c) Plain C/FRT 850°C/Annealed at 740°C for 15 minutes.
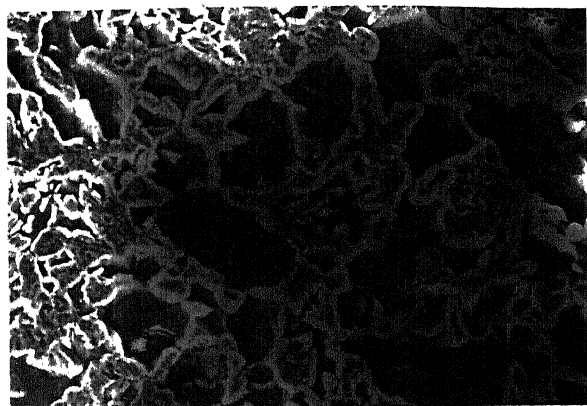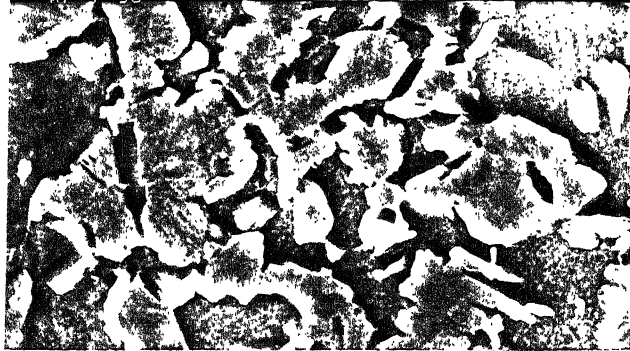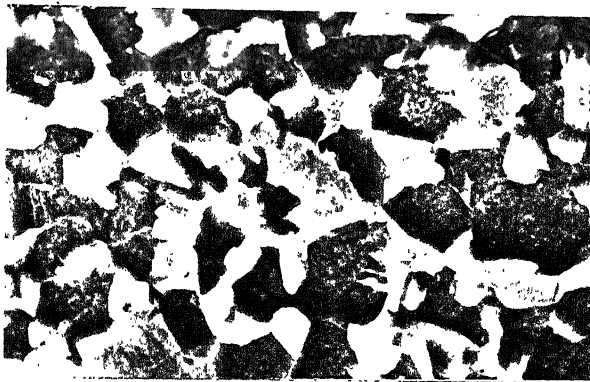(d) Nb Steel/FRT 850°C/Annealed at 740°C for 15 minutes.

(e)

(f)

(g)

(h)

Figure-4.3.1 SEM Micrographs of Plain C and Nb Steels

(e) Plain C/FRT 770°C/Annealed at 740°C for 15 minutes.
(f) Nb Steel/FRT 770°C/Annealed at 740°C for 15 minutes.
(g) Plain C/FRT 730°C/Annealed at 740°C for 15 minutes.
(h) Nb Steel/FRT 730°C/Annealed at 740°C for 15 minutes.

·(i)

(j)

Figure-4.3.1 SEM Micrographs of Plain C and Nb Steels

(i) Plain C/FRT 630°C/Annealed at 740°C for 15 minutes.
(j) Nb Steel/FRT 630°C/Annealed at 740°C for 15 minutes.

(a)

(b)

(c)

(d)

Figure-4.3.2 SEM Micrographs of Plain C and Nb Steels

(a) Plain C/FRT 1020°C/Annealed at 820°C for 15 minutes.
(b) Nb Steel/FRT 1020°C/Annealed at 820°C for 15 minutes.
(c) Plain C/FRT 850°C/Annealed at 820°C for 15 minutes.
(d) Nb Steel/FRT 850°C/Annealed at 820°C for 15 minutes.

(e)

(f)

(g)

(h)

Figure-4.3.2 SEM Micrographs of Plain C and Nb Steels

(e) Plain C/FRT 770°C/Annealed at 820°C for 15 minutes.
(f) Nb Steel/FRT 770°C/Annealed at 820°C for 15 minutes.
(g) Plain C/FRT 730°C/Annealed at 820°C for 15 minutes.
(h) Nb Steel/FRT 730°C/Annealed at 820°C for 15 minutes.

(i)

(j)

Figure-4.3.2 SEM Micrographs of Plain C and Nb Steels

(i) Plain C/FRT 630°C/Annealed at 820°C for 15 minutes.
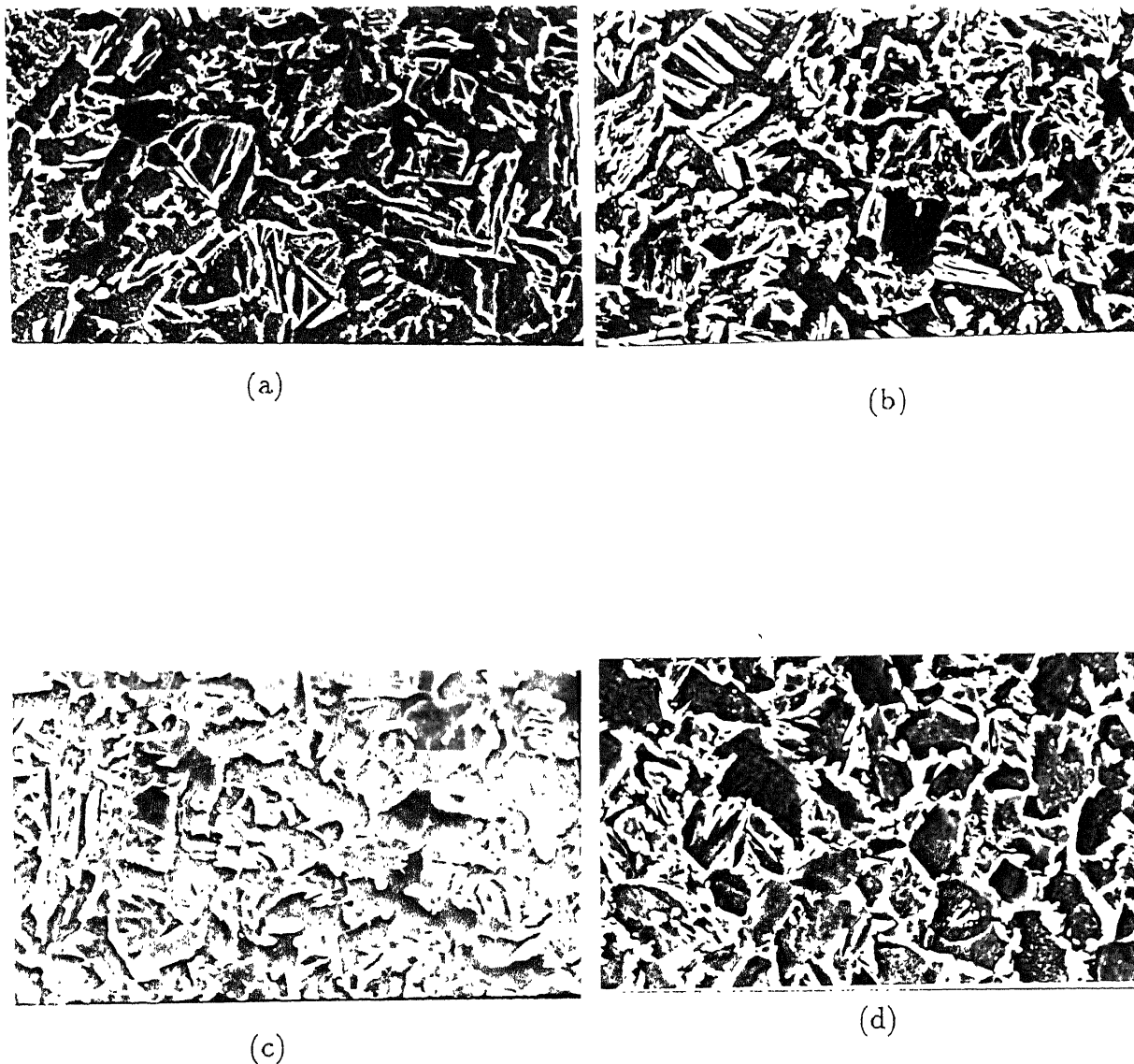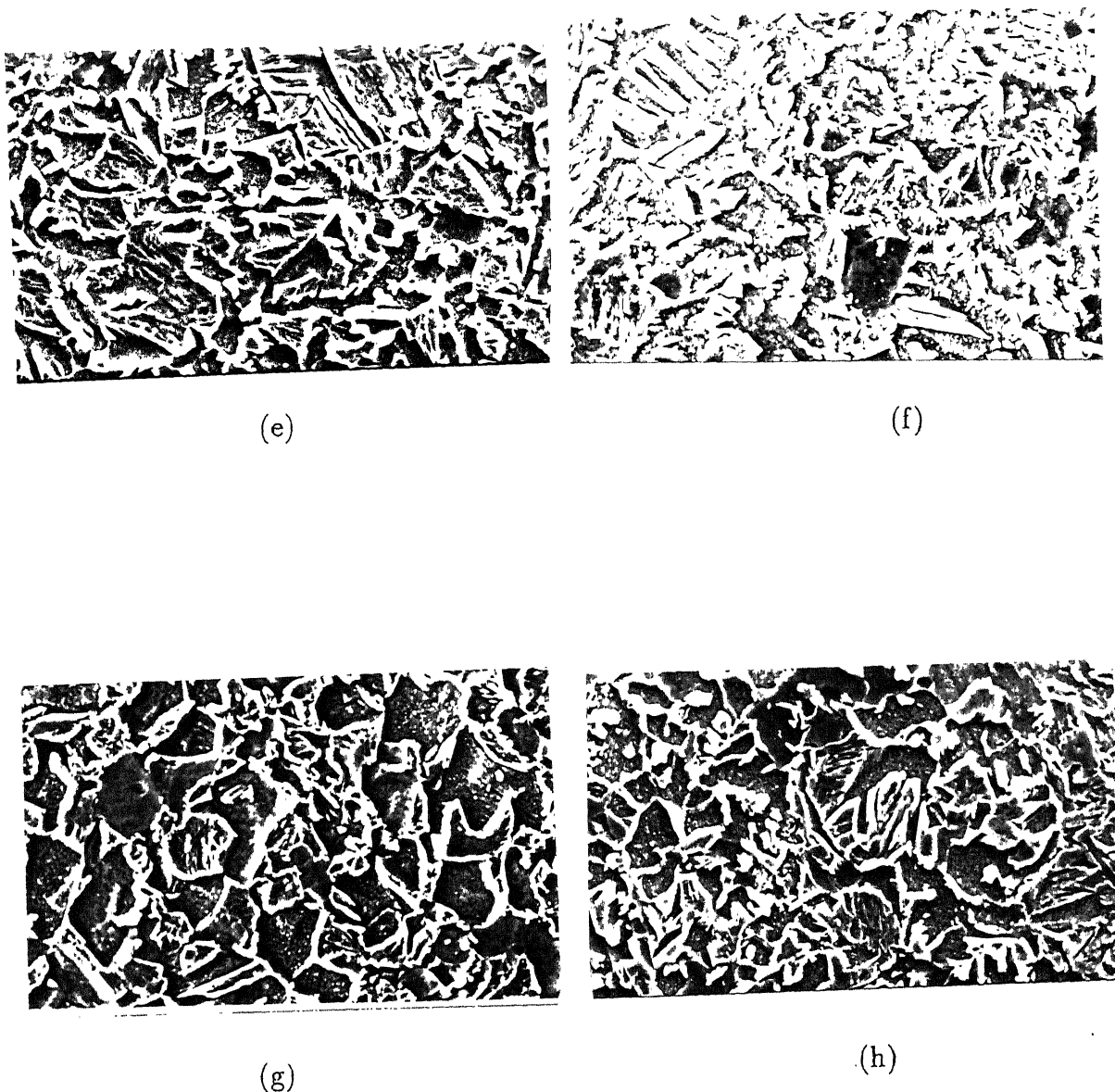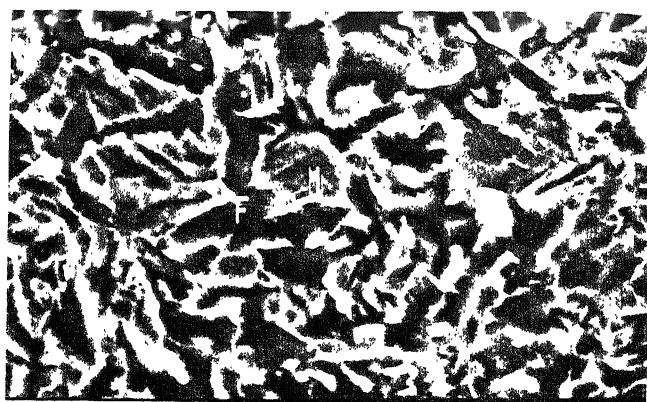(j) Nb Steel/FRT 630°C/Annealed at 820°C for 15 minutes.

TABLE - 4.3.1

As Received Sample	Heat Treatment Schedules	V^m (%)	V^f (%)	N_l^m (10^{-3}) (mm)	σ^m (10^{-3}) (mm)	λ^f (10^{-3}) (mm)	λ^m (10^{-3}) (mm)
Plain C Steel Finish Rolled at 1020°C	740°C/3 mins.	34	66	80	12.50	8.25	4.25
	740°C/15 mins.	45	55	75	13.33	7.33	6.00
	740°C/30 mins.	55	45	69	14.49	6.52	7.97
	740°C/60 mins.	61	39	60	16.67	6.50	10.17
Plain C Steel Finish Rolled at 850°C	740°C/3 mins.	35	65	188	5.32	3.46	1.86
	740°C/15 mins.	43	57	148	6.76	3.85	2.91
	740°C/30 mins.	46	54	125	8.00	4.32	3.68
	740°C/60 mins.	53	47	100	10.00	4.70	5.30
Plain C Steel Finish Rolled at 770°C	740°C/3 mins.	36	64	190	5.26	3.37	1.89
	740°C/15 mins.	42	58	260	3.84	2.23	1.62
	740°C/30 mins.	48	52	206	4.85	2.52	2.33
	740°C/60 mins.	58	42	105	9.52	4.00	5.62
Plain C Steel Finish Rolled at 730°C	740°C/3 mins.	42	58	193	5.18	3.01	2.18
	740°C/15 mins.	46	54	159	6.29	3.40	2.89
	740°C/30 mins.	51	49	116	8.62	4.24	4.40
	740°C/60 mins.	57	43	105	9.52	4.09	5.43
Plain C Steel Finish Rolled at 630°C	740°C/3 mins.	45	55	227	4.41	2.42	1.98
	740°C/15 mins.	50	50	144	6.94	3.47	3.47
	740°C/30 mins.	56	44	130	7.69	3.38	4.31
	740°C/60 mins.	64	36	124	8.06	2.90	5.16

Quantitative Values of the Metallographic Parameters for the Plain C Steel in the Heat Treated Condition
(Annealing Temperature 740 °C)

$V^m \rightarrow$ Volume Fraction of Martensite.

$V^f \rightarrow$ Volume Fraction of Ferrite.

$N_l^m \rightarrow$ Number of Martensite Particles Per Unit Length.

$\sigma^m \rightarrow$ Mean Random Spacing of Martensite Per Unit Length.

$\lambda^f \rightarrow$ Mean Free Path of Ferrite Per Unit Length.

$\lambda^m \rightarrow$ Mean Free Path of Martensite Per Unit Length.

TABLE - 4.3.2

As Received Sample	Heat Treatment Schedules	V^m (%)	V^f (%)	N_l^m (10^{-3}) (mm)	σ^m (10^{-3}) (mm)	λ^f (10^{-3}) (mm)	λ^m (10^{-3}) (mm)
Nb Steel Finish Rolled at 1020°C	740°C/3 mins.	34	66	151	6.62	3.71	2.25
	740°C/15 mins.	46	54	140	7.14	3.86	3.29
	740°C/30 mins.	52	48	71	14.08	6.67	7.32
	740°C/60 mins.	59	41	64	15.63	6.41	9.22
Nb Steel Finish Rolled at 850°C	740°C/3 mins.	35	65	199	5.03	3.27	1.76
	740°C/15 mins.	45	55	139	7.19	3.96	3.24
	740°C/30 mins.	50	50	135	7.41	3.70	3.70
	740°C/60 mins.	54	46	103	9.71	4.47	5.24
Nb Steel Finish Rolled at 770°C	740°C/3 mins.	40	60	190	5.26	3.16	2.11
	740°C/15 mins.	43	57	247	4.05	2.31	1.74
	740°C/30 mins.	47	53	133	8.85	3.98	3.53
	740°C/60 mins.	54	46	183	5.46	2.51	2.95
Nb Steel Finish Rolled at 730°C	740°C/3 mins.	41	59	215	4.65	2.74	1.91
	740°C/15 mins.	48	52	272	3.68	1.91	1.76
	740°C/30 mins.	52	48	115	8.70	4.17	4.52
	740°C/60 mins.	59	41	72	13.88	5.69	8.19
Nb Steel Finish Rolled at 630°C	740°C/3 mins.	42	58	376	2.72	1.54	1.12
	740°C/15 mins.	47	53	294	3.40	1.80	1.60
	740°C/30 mins.	53	47	230	4.35	2.04	2.30
	740°C/60 mins.	60	40	150	6.67	2.67	4.00

Quantitative Values of the Metallographic Parameters for the
Nb Microalloyed Steel in the Heat Treated Condition
(*Annealing Temperature 740 °C*)

$V^m \rightarrow$ Volume Fraction of Martensite.

$V^f \rightarrow$ Volume Fraction of Ferrite.

$N_l^m \rightarrow$ Number of Martensite Particles Per Unit Length.

$\sigma^m \rightarrow$ Mean Random Spacing of Martensite Per Unit Length.

$\lambda^f \rightarrow$ Mean Free Path of Ferrite Per Unit Length.

$\lambda^m \rightarrow$ Mean Free Path of Martensite Per Unit Length.

TABLE - 4.3.3

As Received Sample	Heat Treatment Schedules	V^m (%)	V^f (%)	N_l^m (10^{-3}) (mm)	σ^m (10^{-3}) (mm)	λ^f (10^{-3}) (mm)	λ^m (10^{-3}) (mm)
Plain C Steel Finish Rolled at 1020°C	820°C/3 mins.	50	50	106	9.43	4.72	4.72
	820°C/15 mins.	75	25	99	10.10	2.53	7.58
	820°C/30 mins.	80	20	100	10.00	2.00	8.00
	820°C/60 mins.	90	10	95	10.53	1.05	9.47
Plain C Steel Finish Rolled at 850°C	820°C/3 mins.	43	57	174	5.75	3.28	2.47
	820°C/15 mins.	60	40	145	6.90	2.76	4.14
	820°C/30 mins.	73	27	138	7.25	1.96	5.29
	820°C/60 mins.	85	15	129	7.75	1.16	6.59
Plain C Steel Finish Rolled at 770°C	820°C/3 mins.	65	35	180	5.56	1.94	3.61
	820°C/15 mins.	70	30	148	6.76	2.03	4.73
	820°C/30 mins.	78	22	137	7.30	1.61	5.69
	820°C/60 mins.	90	10	122	8.20	0.82	7.38
Plain C Steel Finish Rolled at 730°C	820°C/3 mins.	63	37	147	6.80	2.52	4.29
	820°C/15 mins.	71	29	126	7.94	2.30	5.63
	820°C/30 mins.	85	15	123	8.13	1.22	6.91
	820°C/60 mins.	93	07	103	9.71	0.68	9.03
Plain C Steel Finish Rolled at 630°C	820°C/3 mins.	54	46	174	5.75	2.64	3.10
	820°C/15 mins.	70	30	135	7.41	2.22	5.19
	820°C/30 mins.	88	12	119	8.40	1.01	7.39
	820°C/60 mins.	96	04	90	11.11	0.44	10.67

Quantitative Values of the Metallographic Parameters for the
Plain C Steel in the Heat Treated Condition
(Annealing Temperature 820 °C)

$V^m \rightarrow$ Volume Fraction of Martensite.

$V^f \rightarrow$ Volume Fraction of Ferrite.

$N_l^m \rightarrow$ Number of Martensite Particles Per Unit Length.

$\sigma^m \rightarrow$ Mean Random Spacing of Martensite Per Unit Length.

$\lambda^f \rightarrow$ Mean Free Path of Ferrite Per Unit Length.

$\lambda^m \rightarrow$ Mean Free Path of Martensite Per Unit Length.

TABLE - 4.3.4

As Received Sample	Heat Treatment Schedules	V^m (%)	V^f (%)	N_l^m (10^{-3}) (mm)	σ^m (10^{-3}) (mm)	λ^f (10^{-3}) (mm)	λ^m (10^{-3}) (mm)
Nb Steel Finish Rolled at 1020°C	820°C/3 mins.	52	48	150	6.67	3.20	3.47
	820°C/15 mins.	70	30	141	7.09	2.13	4.96
	820°C/30 mins.	82	18	130	7.69	1.38	6.31
	820°C/60 mins.	90	10	115	8.70	0.87	7.83
Nb Steel Finish Rolled at 850°C	820°C/3 mins.	43	57	156	6.41	3.65	2.76
	820°C/15 mins.	65	35	120	8.33	5.42	2.92
	820°C/30 mins.	75	25	112	8.93	2.23	6.70
	820°C/60 mins.	82	18	105	9.52	1.71	7.81
Nb Steel Finish Rolled at 770°C	820°C/3 mins.	50	50	170	5.88	2.94	2.94
	820°C/15 mins.	84	16	300	3.33	0.53	2.80
	820°C/30 mins.	90	10	120	8.33	0.83	7.50
	820°C/60 mins.	93	07	105	9.52	0.67	8.86
Nb Steel Finish Rolled at 730°C	820°C/3 mins.	46	54	195	5.13	2.77	2.36
	820°C/15 mins.	63	37	251	3.98	1.47	2.51
	820°C/30 mins.	72	28	145	6.89	1.93	4.96
	820°C/60 mins.	81	19	135	7.41	1.41	6.00
Nb Steel Finish Rolled at 630°C	820°C/3 mins.	48	52	180	5.56	2.89	2.67
	820°C/15 mins.	69	31	183	5.46	1.69	3.77
	820°C/30 mins.	74	26	142	7.04	1.83	5.21
	820°C/60 mins.	88	12	140	7.14	0.86	6.28

Quantitative Values of the Metallographic Parameters for the
Nb Microalloyed Steel in the Heat Treated Condition
(Annealing Temperature 820 °C)

$V^m \rightarrow$ Volume Fraction of Martensite.

$V^f \rightarrow$ Volume Fraction of Ferrite.

$N_l^m \rightarrow$ Number of Martensite Particles Per Unit Length.

$\sigma^m \rightarrow$ Mean Random Spacing of Martensite Per Unit Length.

$\lambda^f \rightarrow$ Mean Free Path of Ferrite Per Unit Length.

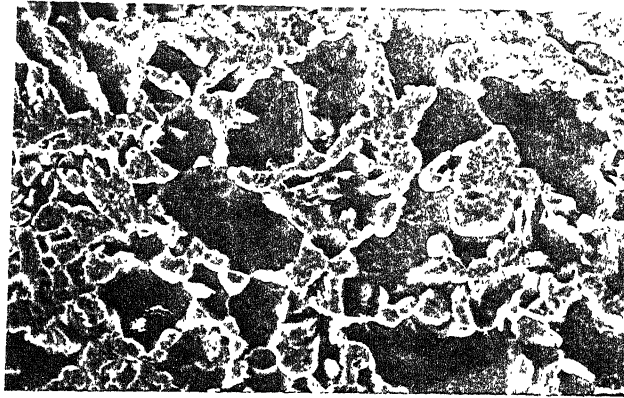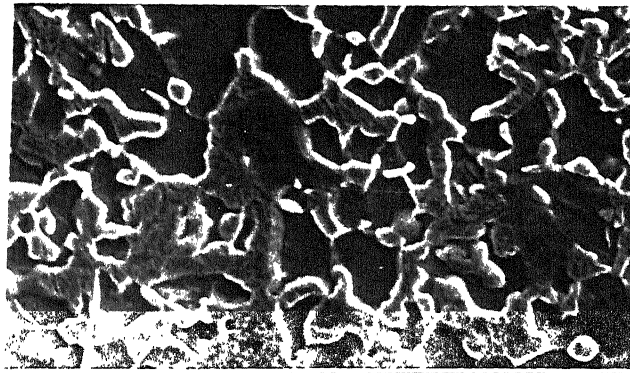$\lambda^m \rightarrow$ Mean Free Path of Martensite Per Unit Length.
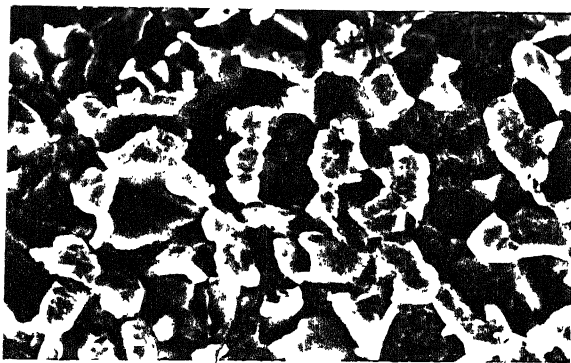
(a)
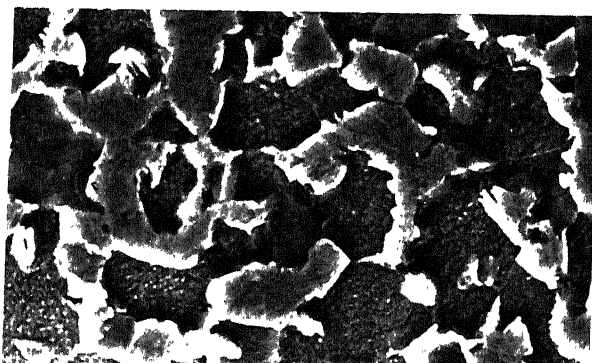
(b).
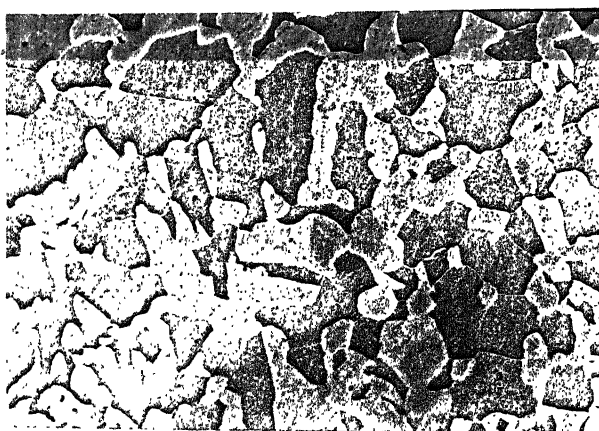
(c)

Figure-4.3.3 Some Selected SEM Micrographs of Plain C and Nb Steel where
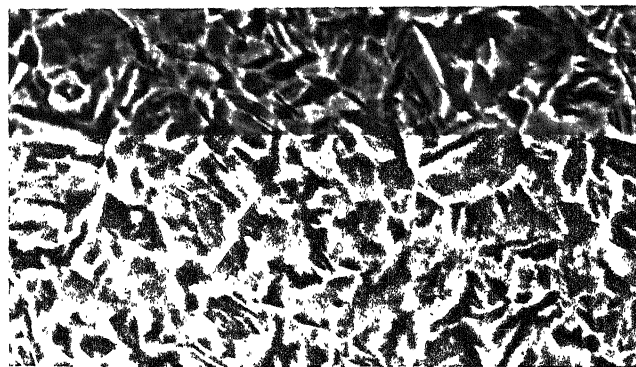Reasonably High Intensity Ratios were Obtained
(a) Nb Steel/FRT 630°C/Annealed at 740°C for 3 minutes.
(b) Plain C/FRT 770°C/Annealed at 740°C for 15 minutes.
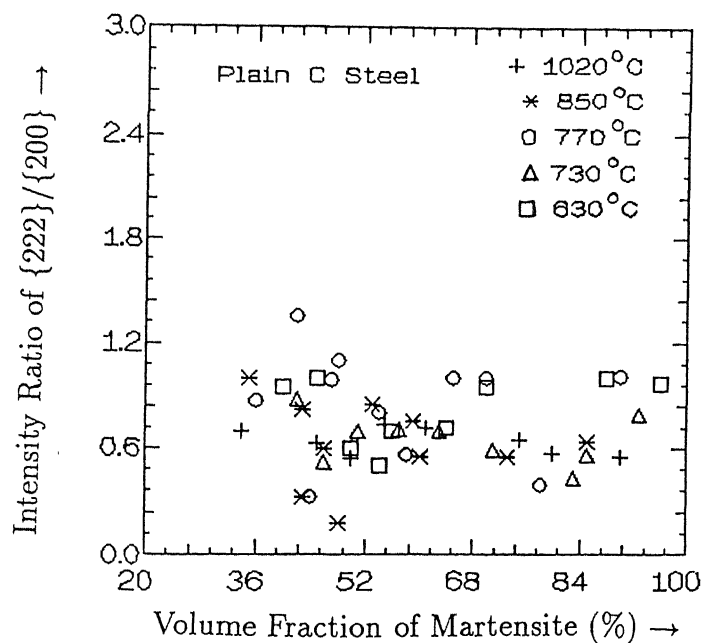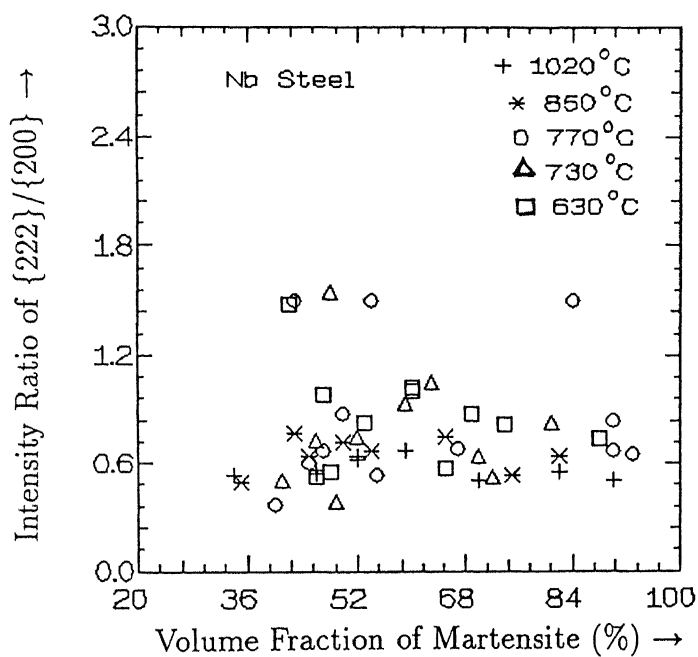(c) Nb Steel/FRT 770°C/Annealed at 740°C for 15 minutes.

(d)

.(e).

(f)

Figure-4.3.3 Some Selected SEM Micrographs of Plain C and Nb Steel where
Reasonably High Intensity Ratios were Obtained
(d) Nb Steel/FRT 730°C/Annealed at 740°C for 15 minutes.
(e) Nb Steel/FRT 770°C/Annealed at 740°C for 60 minutes.
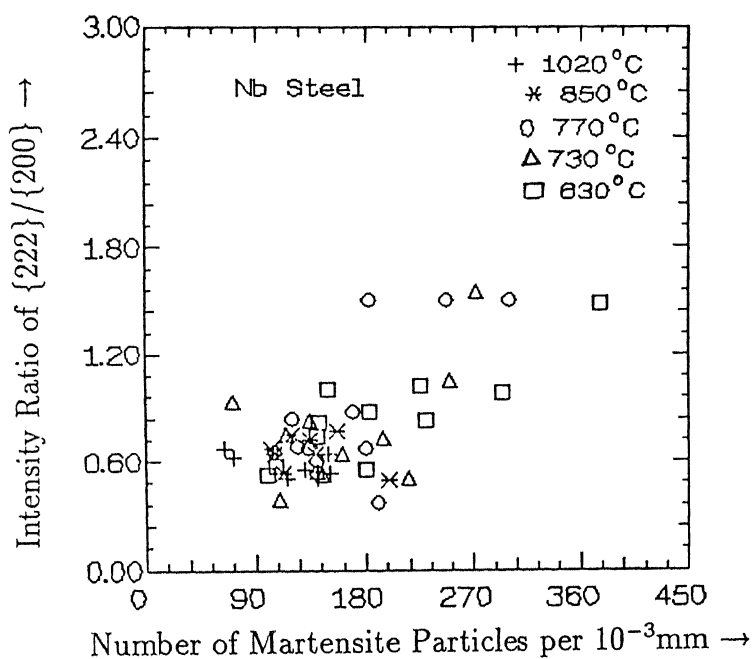(f) Nb Steel/FRT 770°C/Annealed at 820°C for 15 minutes.

(a)

(b)

Figure-4.3.4 {222}/{200} Intensity Ratio vs. Volume Fraction of Martensite (V^m)
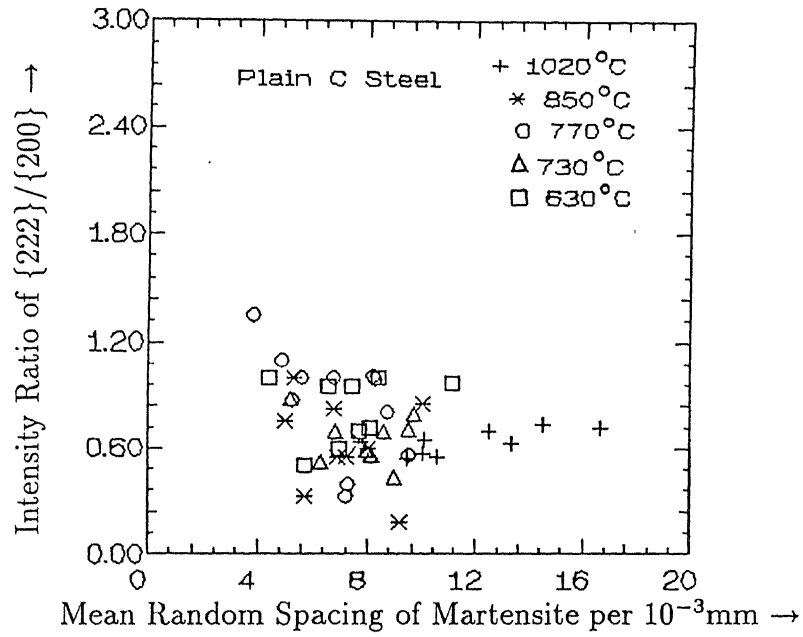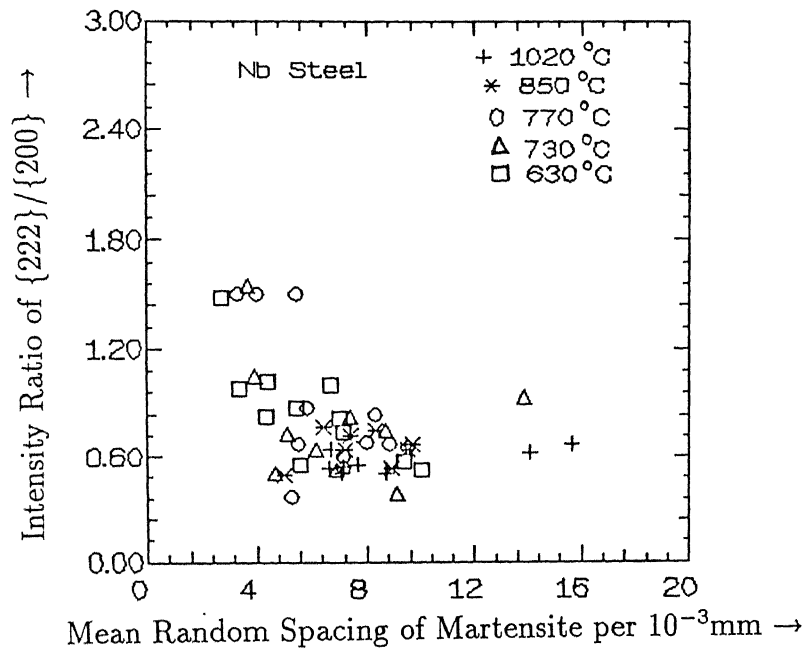for
(a) Plain C Steel
(b) Nb Steel
for all Five FRTs.
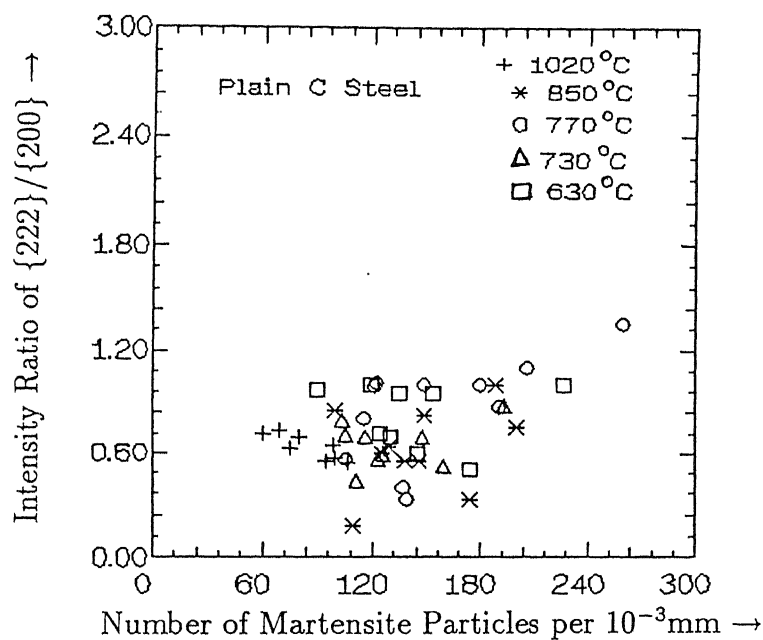
Figure-4.3.5 {222}/{200} Intensity Ratio vs. Number of Martensite Particles per
Unit Length (N_l^m) for
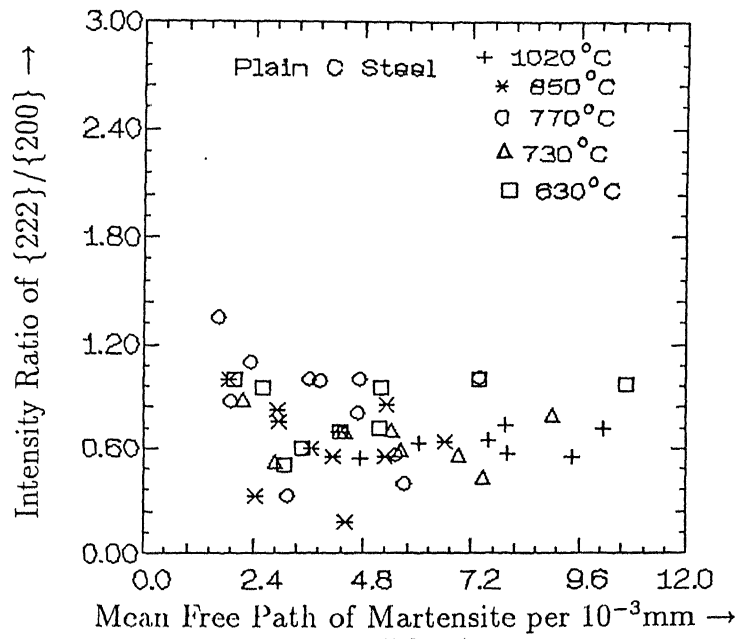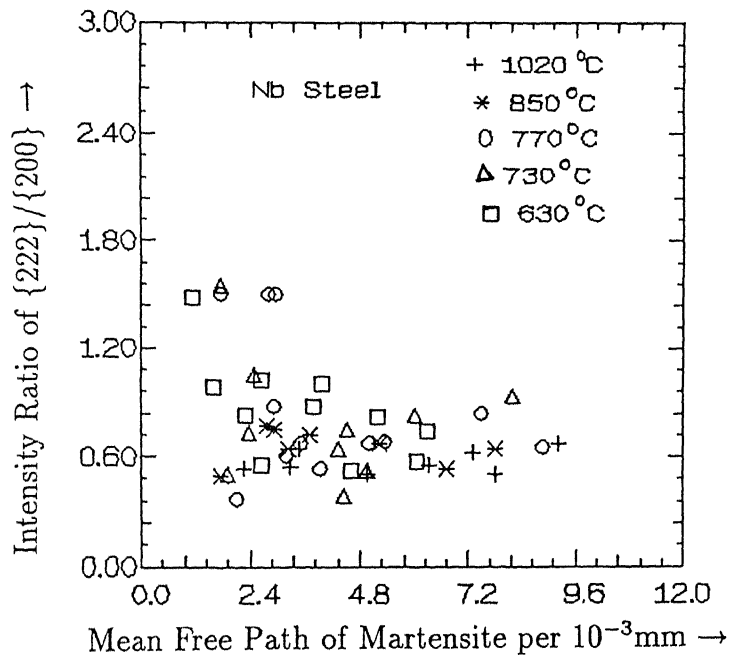(a) Plain C Steel
(b) Nb Steel
for all Five FRTs.

Figure-4.3.6 {222}/{200} Intensity Ratio vs. Mean Random Spacing of Martensite Particles per Unit Length (σ^m) for
(a) Plain C Steel
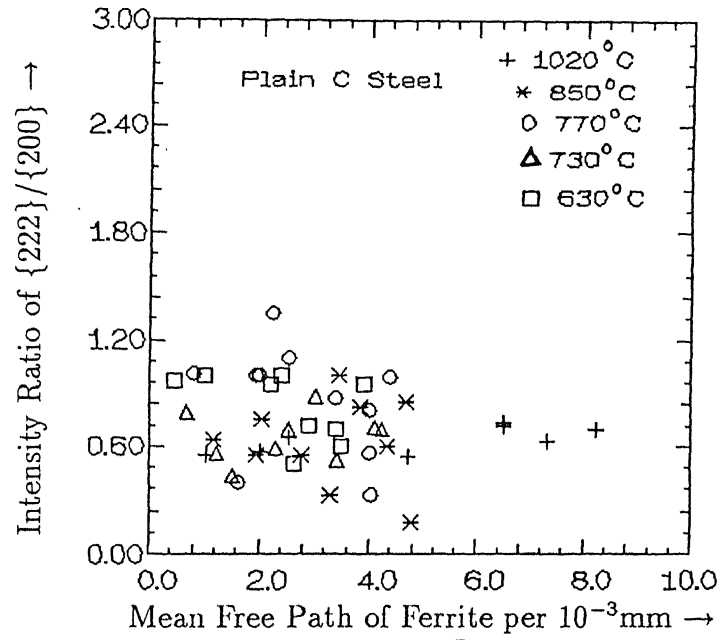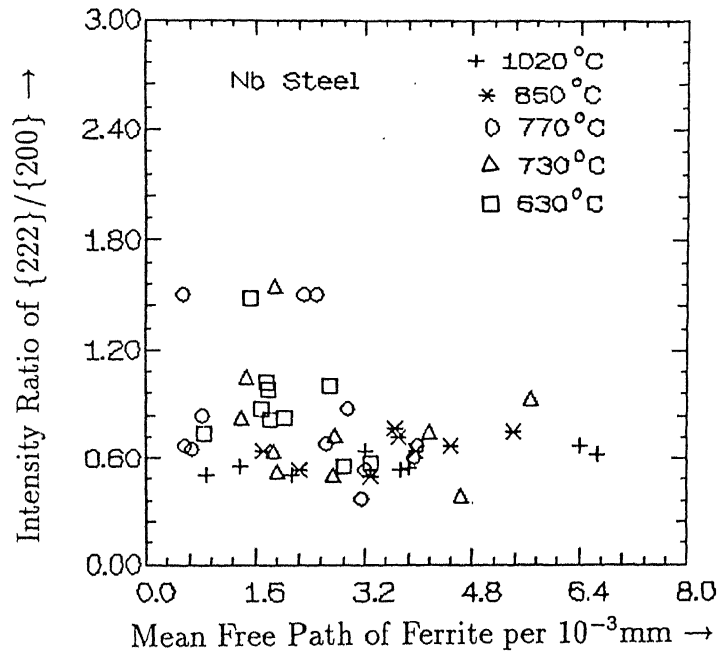(b) Nb Steel
for all Five FRTs.

Figure-4.3.7 {222}/{200} Intensity Ratio vs. Mean Free Path of Martensite
Particles per Unit Length (λ^m) for
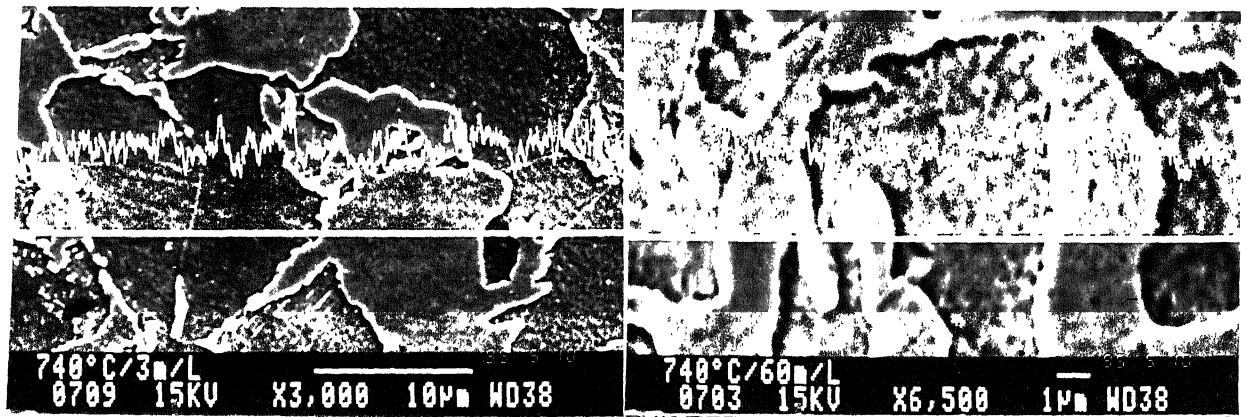(a) Plain C Steel
(b) Nb Steel
for all Five FRTs.

Figure-4.3.8 {222}/{200} Intensity Ratio vs. Mean Free Path of Ferrite per Unit
Length (λ^f) for
(a) Plain C Steel
(b) Nb Steel
for all Five FRTs.

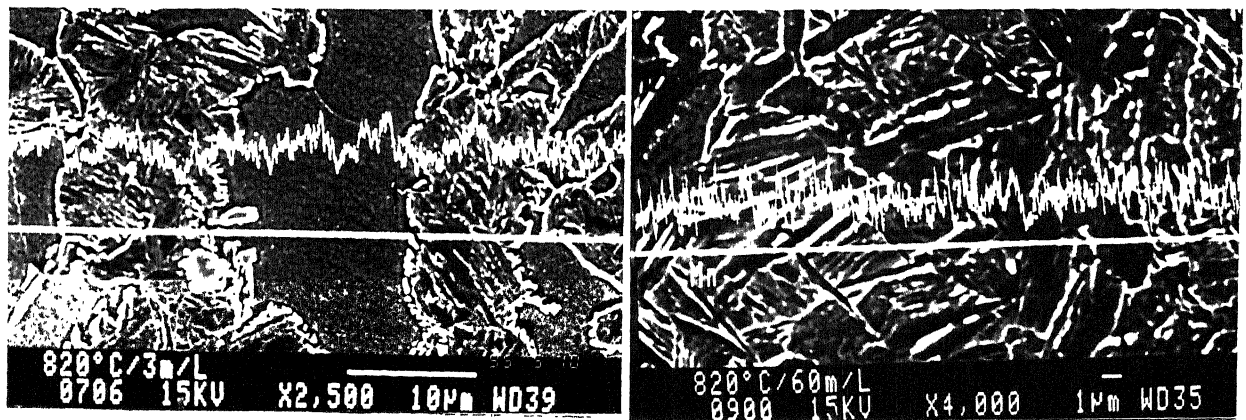Figure-4.4.1 X-ray Line Scan Photographs (Mn K$_\alpha$)
of Plain C Steel
(a) FRT - 1020°C/Annealed at 740°C for 3 mins.
(b) FRT - 1020°C/Annealed at 740°C for 60 mins.
(c) FRT - 1020°C/Annealed at 820°C for 3 mins.
(d) FRT - 1020°C/Annealed at 820°C for 60 mins.

Figure-4.4.2 X-ray Line Scan Photographs (Mn K$_\alpha$)
of Nb Steel
(a) FRT - 1020°C/Annealed at 740°C for 3 mins.
(b) FRT - 1020°C/Annealed at 740°C for 60 mins.
(c) FRT - 1020°C/Annealed at 820°C for 3 mins.
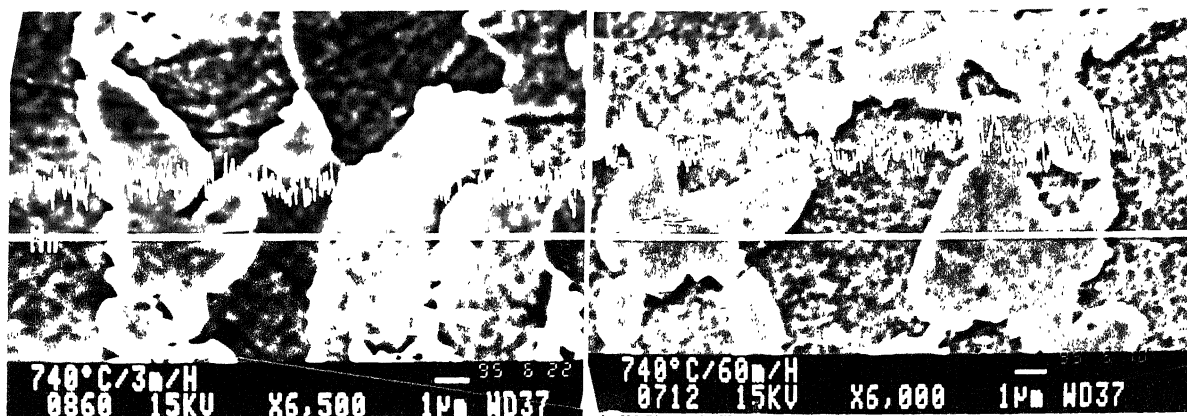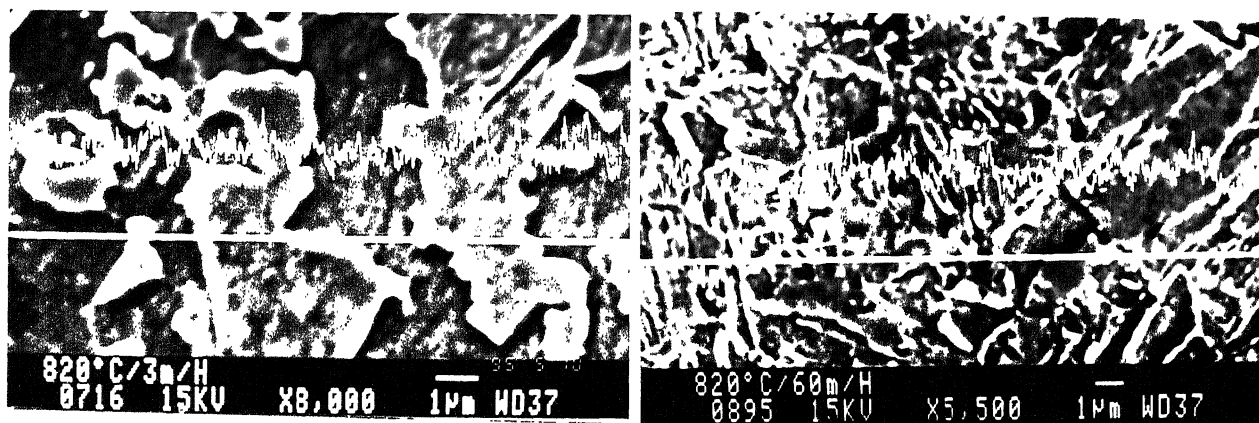(d) FRT - 1020°C/Annealed at 820°C for 60 mins.
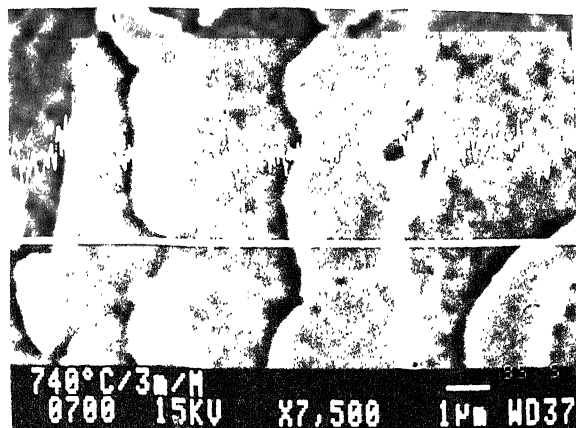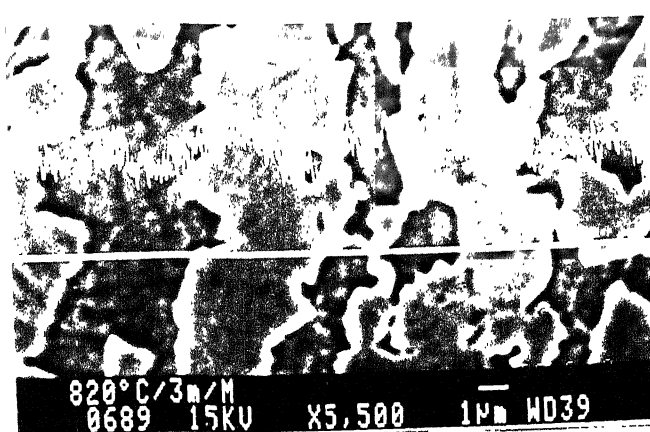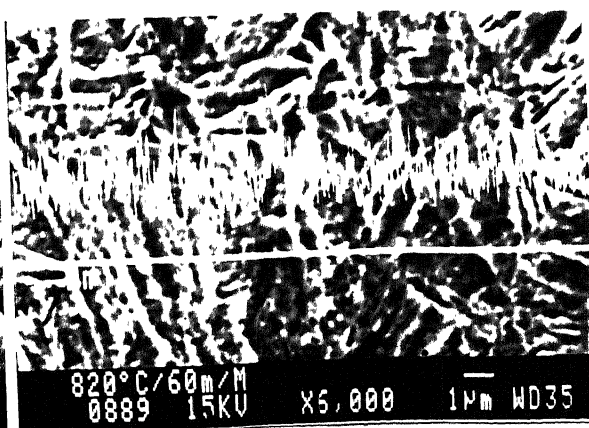
Figure-4.4.3 X-ray Line Scan Photographs (Mn K_α)
of Plain C Steel
(a) FRT - 630°C/Annealed at 740°C for 3 mins.
(b) FRT - 630°C/Annealed at 740°C for 60 mins.
(c) FRT - 630°C/Annealed at 820°C for 3 mins.
(d) FRT - 630°C/Annealed at 820°C for 60 mins.
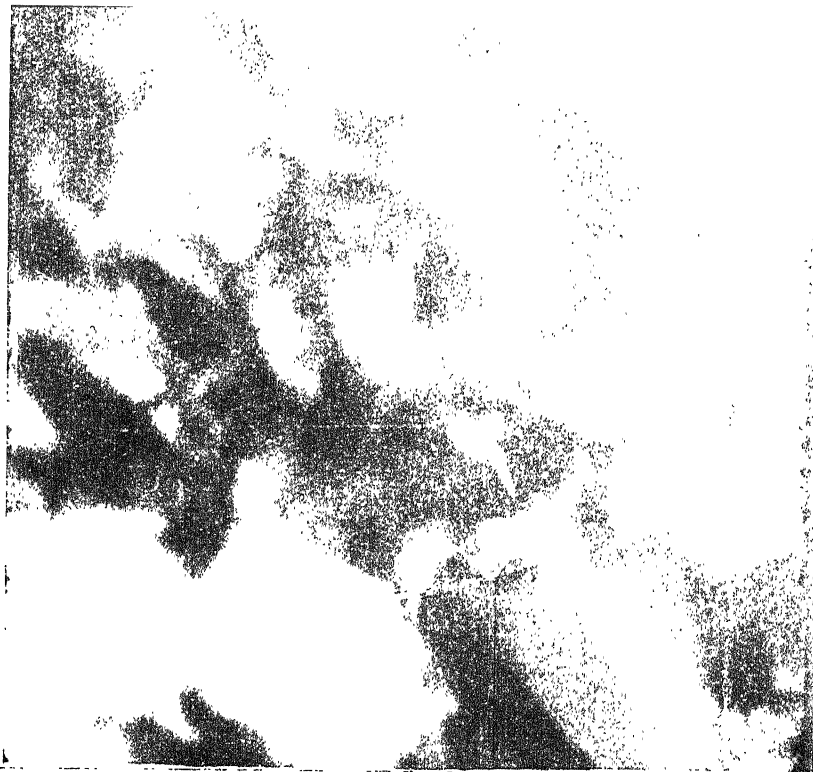
(a)
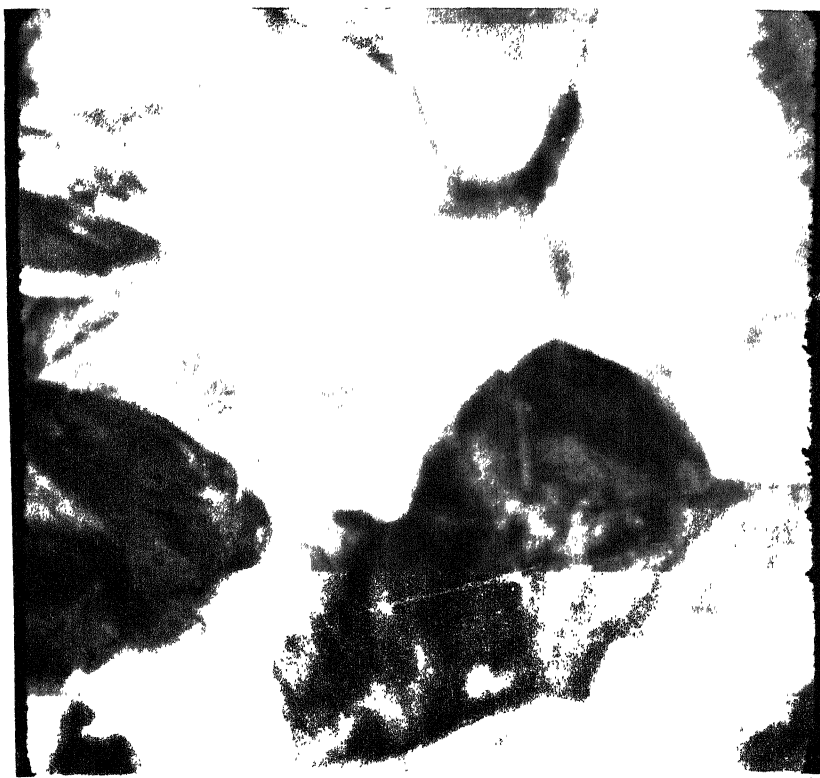
(b)

Figure-4.5.1 TEM Micrographs of Plain C and Nb Steel
(a) Plain C Steel/FRT - 770°C/Annealed at 740°C for 15 mins.
(b) Nb Steel/FRT - 770°C/Annealed at 740°C for 15 mins.

62
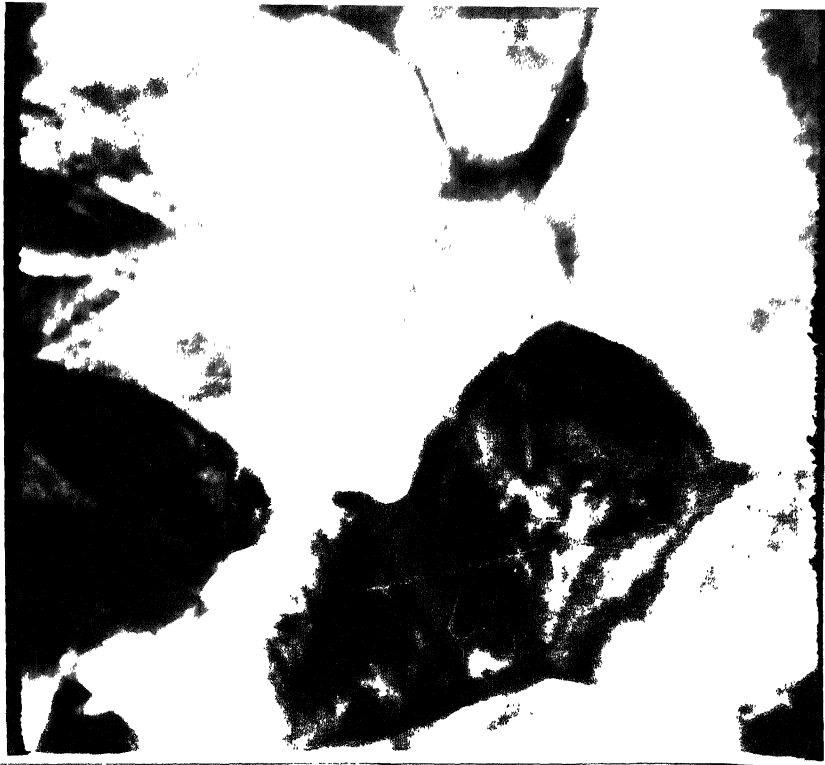
(a)
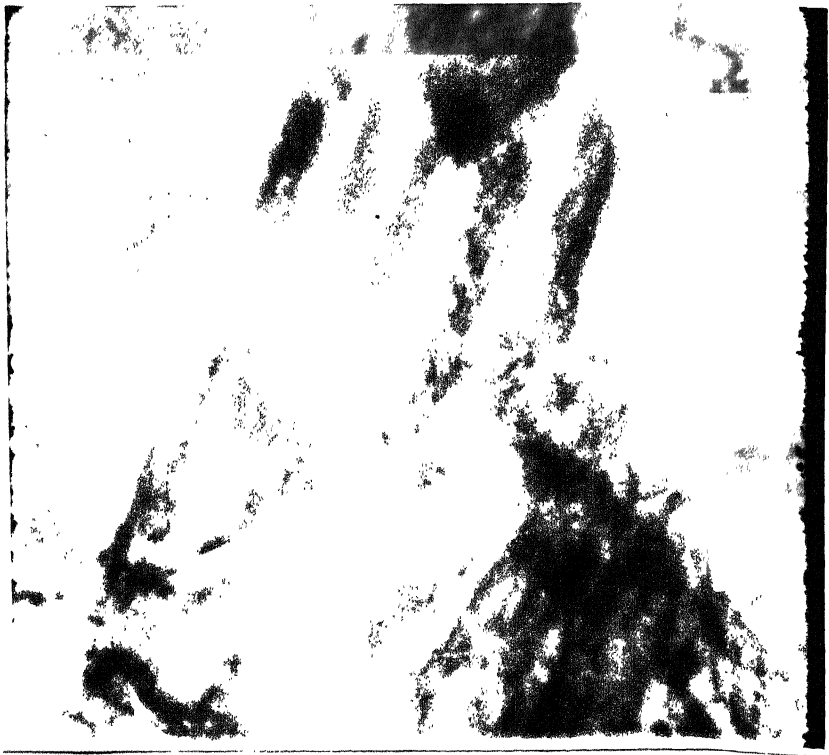
(b).

Figure-4.5.2 TEM Micrographs of Nb Steels
(a) and (b) FRT - 730°C/Annealed at 740°C for 15 mins.
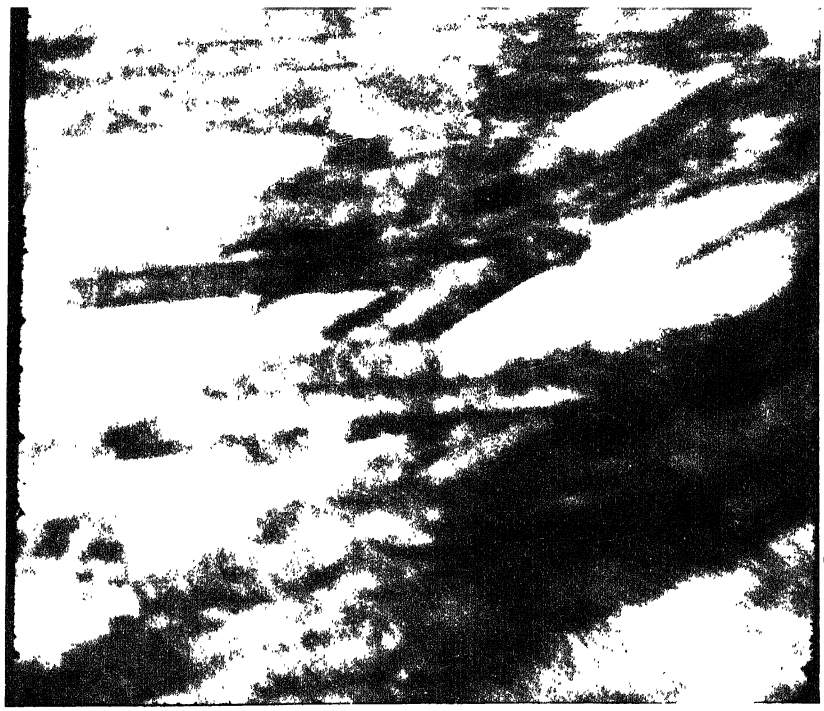
(a)

(b)

Figure-4.5.3 TEM Micrographs of Nb Steel and Plain C Steel
(a) Nb Steel/FRT - 770°C/Annealed at 820°C for 15 mins.
(b) Plain C Steel/FRT - 630°C/Annealed at 820°C for 30 mins.

CHAPTER-5

DISCUSSION

The aim of the present investigation was to correlate deep drawability (measured in terms of $\{222\}/\{200\}$ X-ray intensity ratio) of two steels (a Plain C and another Nb microalloyed) with the metallographic features present in their microstructures. The rationale behind using the $\{222\}/\{200\}$ intensity ratio was the fact that the mean plastic strain ratio (r_m) is directly proportional to this ratio [Figure 1.2]. Reasonably high values of $\{222\}/\{200\}$ were obtained only in a few particular cases. These have not been found strictly to depend on the finish rolling temperature (FRT). However, the highest values were most of the times obtained when the FRT was within the intercritical ($\alpha + \gamma$) region. High values of the ratio were obtained also in case of the sample finish rolled at 630°C (upper α range). Thus finish rolling at temperature 1020°C (in the γ recrystallisation range) or at 850°C (in the γ no-recrystallisation range) were not found to be beneficial at all.

A difference in the value of $\{222\}/\{200\}$ intensity ratio peaks was observed between the rolling and the mid planes of the samples [Tables 4.2.1 to 4.2.5]. In most of the cases it was seen that the intensity ratio values were higher on the rolling plane than on the mid plane. Only in few cases it could be seen that the intensity ratio on mid plane was higher than on the rolling plane; however, this result doesn't seem to be so significant.

The Nb steels exhibited the highest or nearly the highest ($\sim$1.5) intensity ratio values. Only in one case the plain C steel exhibited reasonably high intensity ratio ($\sim$1.35). Based on these observations, the Nb steel can be found to be more appropriate as compared to the plain C steel for deep drawing purpose.

The variation in X-ray intensity ratio values with finish rolling temperature [FRT] for different heat treatment schedules did not reveal any proper correlation between the intensity ratio $\{222\}/\{200\}$ with finish rolling temperature and post rolling annealing schedule. This was found to be true for both the plain C and the Nb steel. In order to examine the correlation between microstructure and texture which is appropriate for better deep drawability, extensive quantitative metallography was done.

Earlier it was believed that high percentage of martensite is not at all beneficial for achieving high r_m value in dual phase steels. Hu [57] has shown that reasonably high r_m value ($\sim$1.8) could be obtained when the martensite volume percent was not more than 4%. Kurihara et. al. [56] reported that the r_m value decreases with martensite volume percent and the proximity between the martensite island. The present results have shown that X-ray intensity ratios are not solely dependent on the volume fraction of martensite of the dual phase steel. In fact, more or less similar volume fraction of martensite could be obtained in both the steels just by changing the heat treatment

schedules. However, X-ray intensity ratio values were observed to be quite different even though the volume fraction of martensite particles were more or less same in different samples. Quantitative metallographic observations show that the highest or nearly the highest intensity ratios were obtained in samples where the volume fraction of martensite was reasonably high (about 40 to 50%). In one case the volume fraction of martensite was as high as $\sim 85\%$, although the X-ray intensity ratio was ~ 1.5. So it is not always true that only very low volume fraction of martensite is beneficial for achieving high r_m value.

In addition to the volume fraction of martensite, the number of martensite particles per unit length also appears to be one of the determining factors for the high intensity ratio values. Figures 4.3.5 (a) and (b) clearly reveal that the intensity ratio increases with the number of the martensite particles per unit length. So more number of the martensite particles is one of the beneficial factors for high $\{222\}/\{200\}$ ratios, hence for the high deep drawability of dual phase steels. These results can be coupled with the results shown in Figures 4.3.7 (a) and (b) which indicate that higher intensity ratios can be achieved when the mean free path of martensite (or martensite particle size) is small. So, the conditions under which high intensity ratio can be obtained are that the martensite particle size should be fine and these should be present in the form of a dense aggregate. This implies that the smaller spacing between the martensite particles should give rise to higher intensity ratio. This point is amply illustrated by the results depicted in Figures 4.3.6 (a) and (b).

The mean free path of the ferrite also affects the intensity ratio value (and therefore the r_m value). Though in the Figure 4.3.8 (a), which is for the plain C steel, all the points are clustered together, still there is a slight tendency of the intensity ratio to be higher for the smaller value of the mean free path of ferrite. This effect is more prominent in case of the Nb steel [Figure 4.3.8 (b)].

On the basis of the results stated above, it is clear that the volume fraction of martensite only is not the determining factor for the X-ray intensity ratio. The number of martensite particles per unit length, mean random spacing of the martensite particles, mean free path of the ferrite and the martensite particle size etc. also contribute significantly to the X-ray intensity ratios. Prior to the present investigation, there has been no systematic quantitative metallographic work done to correlate the dual phase microstructures with the intensity of the $\{111\}$ texture.

Another important information from this investigation was that there was significant inhomogeneity of the $\{111\}$ texture on the rolling and the mid plane of the samples after controlled rolling, as well as after dual phasing treatment of the samples. The reason for this difference could not be inferred at the moment and this can only be found out when detailed pole figures and ODFs are determined for the various samples to have an unambiguous idea about the texture present.

CHAPTER-6

CONCLUSIONS

1. Intercritical annealing of two steels (Plain C and Nb microallyed) at 740°C and 820°C for 3, 15, 30 and 60 minutes followed by water quenching produces dual phase (ferrite-martensite) structures with different volume fractions of martensite.

2. The volume fraction of martensite (V^m) increases with the holding time and temperature of annealing.

3. The number of martensite particles per unit length (N_l^m) decreases with the holding time at a particular annealing temperature due to its coarsening. The mean random spacing of the martensite particles per unit length (σ^m) increases with the holding time.

4. The mean free path of martensite (λ^m) increases, whereas the mean free path of ferrite (λ^f) decreases with the holding time for a particular annealing temperature.

5. Different values of {222}/{200} ratio obtained on the rolling and mid planes of many samples suggest inhomogeneity of the rolling deformation along the through thickness direction.

6. Generally the Nb steel shows the highest or nearly the highest intensity ratios of the {222}/{200} peaks. Also the Nb steel samples finish rolled at the intercritical ($\alpha + \gamma$) region or the upper ferrite (α) region appear to possess better deep drawing property. Finish rolling at the γ recrystallisation range is not at all beneficial.

7. The volume fraction of martensite does not appear to be the factor which governs the X-ray intensity ratios. The {222}/{200} X-ray intensity ratio increases as the number of the martensite particles per unit length (N_l^m) increases but the reverse is true for the mean random spacing of martensite per unit length (σ^m). Again, lower is the value of mean free path of ferrite (λ^f) and martensite (λ^m) higher is the value of the X-ray intensity ratio.

8. There appears to be only a slight partitioning of Mn between the ferrite and the austenite (martensite) phases during heat treatment.

9. In case of the Plain C steel, only lath type martensite is found to be present, while both lath type and twinned martensite appear in the Nb steel. The dislocation densities in the ferrite regions adjacent to the martensitic areas are perceptibly higher in the Nb steel as compared to the Plain C steel.

REFERENCES

1. S.Hayami and T.Furukawa : *Microalloying '75*, 1, (1977), 78 New York, Union Carbide corporation.

2. F.B.Picaring : *Microalloying '75*, 1, (1977), 3.

3. T. Gladman; O.David and I.D.McIvor : *Microalloying '75*, 1, (1977), 25.

4. W.S.Owen : *Metall. Ital.*, 75, (1977) 293.

5. T.Matsuoka and K. Yamamori : *Met. Trans. A*, Vol. 6A, Aug. (1975), 1613.

6. M.S.Rashid : *SAE Paper 760206* (1976) and General Motors Research Publication Nos. GMR 2044, 2326, 2413, 2647.

7. W.C.Jeong and C.H.Kim : *Met. Trans. A*, Vol. 18A, May (1987), 933-36.

8. S.Hayaami and T.Furukawa : *Microalloying '75 Procedings*, Washington D.C., Oct. (1975), 311.

9. R.G.Davis : *Met. Trans. A*, Vol. 9A, (1978), 41-52.

10. J.Y.Koo and G.Thomas : *Met. Trans. A*, Vol. 8A, (1977), 525-28.

11. M.S.Rashid : *SAE Trans*, Vol. 86, (1977), 935.

12. J.W.Morrow; A.P.Coldren and G.Tither : *Climax Molybdenum Co.*, Reports L-176-165, L-176-166, (1976).

13. G.Tither; A.P.Coldren and J.W.Morrow : Proc. 20th Mech. Working Conf., Chicago, III (1978).

14. J.W.Morrow and G.Tither : *J. Met.*, Vol. 12, (1978), 20.

15. R.G.Davis : *Met. Trans. A*, Vol. 9A, (1978), 451.

16. R.G.Davis : *Met. Trans. A*, Vol. 9A, (1978), 671.

17. R.G.Davis : *Met. Trans. A*, Vol. 10A, (1979), 113.

18. R.G.Davis : *Met. Trans. A*, Vol. 10A, (1979), 1549.

19. A.R.Marder : *Met. Trans. A*, Vol. 13A, Jan. (1982), 85.

20. A.P.Coldren and G.Tither : *J. Met.*, 4, (1978), 6.

21. T.Furukawa; H.Morikawa; H.Takechi and Koyama : *'Process Factors for Highly Ductile Dual Phase Sheet Steels'*, Report from Research Lab., Nippon Steel Corp., Kawasaki, Japan.

22. E.C.Bain and H.W.Paxton : *'Alloying Elements in Steels'*, 2nd Ed., ASM, Ohio (1966).

23. P.R.Mould and C.C.Skena : *'Formable HSLA and Dual Phase Steels'*, (A.T.Davenport, Ed.) AIME, New York (1977) 181.

24. T.Tanaka; M.Nishida; K.Hashiguchi and T.Kato : *'Structure and Properties of Dual Phase Steels'*, (R.A.Kot and J.W.Morris, Eds.), AIME, New York, (1979) 221.

25. J.M.Grey and R.B.G.Yoo : *Trans. A.S.M*, 61, (1968), 255.

26. R.W.K.Honeycombe : *Structure and Strength of Alloy Steels*, 1974, Climax Molybdenum Co. Publ.

27. G.F.Bolling and R.H.Richman : *Canadian J. Phys.*, 45, (1967), 541.

28. H.Masui and H.Takechi : *Trans. ISIJ*, 16, (1976), 69.

29. S.Takeuchi; T.Taoka and H.Yoshida : *Trans. ISIJ*, 9, (1969), 105.

30. P.M.Kelly and J.Nutting : *ISIJ*, 197, (1961), 199.

31. J.H.Bucher and E.G.Hamburg : *SAE Paper 770164*, 1977.

32. A.P.Coldren; G.Tither; A.Conford and J.R.Hiam : *'Formable HSLA and Dual Phase Steels'*, (A.T.Davenport, Ed.), AIME, New York, (1977), 701.

33. K.W.Andrews : *J. Iron Steel Inst.*, London, 203, (1965), 721.

34. M.O.Geib; D.K.Matlock and G.Krauss : *Met. Trans. A*, Vol. 11A, (1980), 1683.

35. C.A.Siebert; D.V.Doane and D.H.Breen : *'The Hardenability of Steels'*, ASM, Metals Park, Ohio (1977).

36. G.S.Huppi; D.K.Matlock and G.Krauss : *Scripta Met.*, 14, (1980), 1239.

37. A.Nakagawa; J.Y.Koo and G.Thomas : *Met. Trans. A*, Vol. 12A, (1988), 1965.

38. G.Tither; A.P.Coldren and J.W.Morrow : Climax Molybdenum Co. Report L-176-163 (1976).

39. N.J.Kim and G.Thomas : *Met. Trans. A*, Vol. 12A, (1981), 483.

40. J.M.Rigsbee and P.J.Van der Arend : *'Formable HSLA and Dual Phase Steels'*, (A.T.Davenport, Ed.), AIME, New York, (1977), 56.

41. A.R.Marder : *'Formable HSLA and Dual Phase Steels'*, (A.T.Davenport, Ed.), AIME, New York, (1977), 87.

42. R.Stevenson; D.J.Bailey and G.Thomas : *Met. Trans. A*, 10A, (1979), 47.

43. J.H.Hollomon : *Trans. AIME*, 162, (1945), 268.

44. P.Ludwik : *Elements der Technologischem Mechanik*, Julius Springer, Berlin, (1909), 32.

45. M.S.Rashid : *'Formable HSLA and Dual Phase Steel'*, (A.T.Davenport, Ed.), AIME, New York, (1977), 1.

46. I.L.Dillamore; K.I.Nam and M.B.O.O.Shitta : 3rd *Congresso Brasileiro de Engenharia e Ciencia dos Materials*, Dec. (1978).

47. L.F.Ramos; D.K.Matlock and G.Krauss : *Met. Trans. A*, 14A, Jul. (1983), 1497-04.

48. C.Crussard : *Rev. Met.*, Paris, France, 10, (1953), 697.

49. B.Jaoult : *J. Mech. and Phys. Solids*, 5, (1957), 95.

50. S.N.Monteiro and R.E.Reed-hill : *Met. Trans.*, 2, (1971), 2947-49.

51. J.Gurland : *Mat. Sci. Eng.*, 13, (1979), 59-71.

52. D.L.Bourell and A.Rizk : *Acta. Metall.*, Vol. 31(4), (1983), 609-17.

53. R.G.Davis and C.L.Magee : *J. Metals*, Nov. (1979), 17-23.

54. W.T.Lankford : *Trans. ASM*, 42, (1950), 1192.

55. M.B.O.O.Shitta : *Ph.D. Thesis, Univ. of Aston*, Birmingham, (1981).

56. K.Kurihara; Y.Hosoya and K.Nakaoka : Proc. 6th Int. Conf. *'Texture of Materials'*, Tokyo, (1981).

57. H.Hu : *Met. Trans. A*, 13A, (1982), 1257.

58. W.B.Hutchinson : *Sheet Met. Ind.*, (1983), 502.

59. B.D.Cullity : *Elements of X-ray Diffraction*, Addison-Wesley, 2nd Ed. (1978).

60. H.J.Bunge : *Z. Metalkd*, 56, (1965), 872.

61. R.J.Roe : *J. Appl. Phys.*, 36, (1965), 2024.

62. J.Hansen; J.Pospiech and K.Lücke : *Table for Texture Analysis of Cubic Crystals*, Springer Verlag, Berlin, (1978).

63. R.K.Ray : *Scripta Met.*, 11, (1984), 1211.

64. H.J.Bunge; C.M.Vlad and H.Kopp : *Archiv für Eisenhüttenwesen*, 55, (1984), 163.

65. H.J.Bunge; C.M.Vlad : Proc. 6th Int. Conf. on *'Texture of Materials'*, 7, (1951), 649, Tokyo, The Iron & Steel Inst. Of Japan.

66. H.Hu : *Formable HSLA and Dual Phase Steels*, (A.T.Davenport, Ed.), Conf. Proc., TMS-AIME, (1979), 109-25.

67. R.K.Ray : *J. Mat. Sci. Lett.*, 4, (1985), 67.

68. D.K.Mondal and R.K.Ray : *Textures and Microstructures*, 21, (1993), 39-53.

69. W.R.Cribb : *Scripta Met.*, 12, (1978), 893.

70. R.L.Lawson; D.K.Matlock C.Krauss : *Metallography*, 13, (1980), 71.

71. N.Pussegoda *et. al* : *Met. Trans. A*, 15A, July (1984), 1499.

72. R.G.Davies and C.L.Magee : *Unpublished Work*.

73. M.Hatherly and W.B.Hutchinson : *An Introduction to Textures in Metals*, The Inst. of Metallurgists, Mon. No. 5, (1979), 6.

74. H.J.Bunge : *Mathematische Methoden der Texturanalyse*, Akademieverlag, Berlin (1969).

75. J.Savoie; R.K.Ray; M.P.Butron-Guillen and J.J.Jonas : *Acta Metall.*, 42(7), (1994), 2511.

76. J.F.Held : *'Mechanical Working and Steel Processing-IV*, (Ed. D.A.Edgecombe), 3, (1965), New York.

A121240

MME-1996-M-RAC-GTR